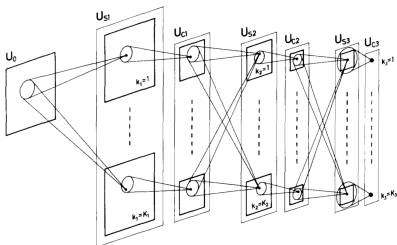


The Little Book of Deep Learning

François Fleuret



UNIVERSITÉ
DE GENÈVE

[François Fleuret](#) is a professor of computer science at the University of Geneva, Switzerland.

The cover illustration is a schematic of the Neocognitron by [Fukushima \[1980\]](#), a key ancestor of deep neural networks.

This ebook is formatted to fit on a phone screen.

Contents

| | |
|---------------------------------------|-----------|
| Contents | 5 |
| List of figures | 7 |
| Foreword | 8 |
| I Foundations | 10 |
| 1 Machine Learning | 11 |
| 1.1 Learning from data | 12 |
| 1.2 Basis function regression | 14 |
| 1.3 Under and overfitting | 16 |
| 1.4 Categories of models | 18 |
| 2 Efficient Computation | 20 |
| 2.1 GPUs, TPUs, and batches | 21 |
| 2.2 Tensors | 23 |
| 3 Training | 25 |
| 3.1 Losses | 26 |
| 3.2 Autoregressive models | 30 |
| 3.3 Gradient descent | 35 |

| | | |
|------------|-----------------------------------|------------|
| 3.4 | Backpropagation | 40 |
| 3.5 | The value of depth | 45 |
| 3.6 | Training protocols | 48 |
| 3.7 | The benefits of scale | 52 |
| II | Deep Models | 57 |
| 4 | Model Components | 58 |
| 4.1 | The notion of layer | 59 |
| 4.2 | Linear layers | 61 |
| 4.3 | Activation functions | 71 |
| 4.4 | Pooling | 74 |
| 4.5 | Dropout | 77 |
| 4.6 | Normalizing layers | 80 |
| 4.7 | Skip connections | 84 |
| 4.8 | Attention layers | 87 |
| 4.9 | Token embedding | 95 |
| 4.10 | Positional encoding | 96 |
| 5 | Architectures | 98 |
| 5.1 | Multi-Layer Perceptrons | 99 |
| 5.2 | Convolutional networks | 101 |
| 5.3 | Attention models | 108 |
| III | Applications | 116 |
| 6 | Prediction | 117 |
| 6.1 | Image denoising | 118 |
| 6.2 | Image classification | 120 |
| 6.3 | Object detection | 121 |

| | | |
|-------------------------|----------------------------------|------------|
| 6.4 | Semantic segmentation | 126 |
| 6.5 | Speech recognition | 129 |
| 6.6 | Text-image representations . . . | 131 |
| 6.7 | Reinforcement learning | 134 |
| 7 | Synthesis | 138 |
| 7.1 | Text generation | 139 |
| 7.2 | Image generation | 142 |
| 8 | The Compute Schism | 146 |
| 8.1 | Prompt Engineering | 147 |
| 8.2 | Quantization | 150 |
| 8.3 | Adapters | 153 |
| 8.4 | Model merging | 156 |
| The missing bits | | 158 |
| Bibliography | | 164 |
| Index | | 176 |

List of Figures

| | | |
|------|--|----|
| 1.1 | Kernel regression | 14 |
| 1.2 | Overfitting of kernel regression | 16 |
| 3.1 | Causal autoregressive model | 32 |
| 3.2 | Gradient descent | 36 |
| 3.3 | Backpropagation | 40 |
| 3.4 | Feature warping | 46 |
| 3.5 | Training and validation losses | 49 |
| 3.6 | Scaling laws | 53 |
| 3.7 | Model training costs | 55 |
| 4.1 | 1D convolution | 63 |
| 4.2 | 2D convolution | 64 |
| 4.3 | Stride, padding, and dilation | 65 |
| 4.4 | Receptive field | 68 |
| 4.5 | Activation functions | 72 |
| 4.6 | Max pooling | 75 |
| 4.7 | Dropout | 78 |
| 4.8 | Dropout 2D | 79 |
| 4.9 | Batch normalization | 81 |
| 4.10 | Skip connections | 85 |

| | | |
|------|---|-----|
| 4.11 | Attention operator interpretation | 88 |
| 4.12 | Complete attention operator | 90 |
| 4.13 | Multi-Head Attention layer | 92 |
| 5.1 | Multi-Layer Perceptron | 99 |
| 5.2 | LeNet-like convolutional model | 102 |
| 5.3 | Residual block | 103 |
| 5.4 | Downscaling residual block | 104 |
| 5.5 | ResNet-50 | 105 |
| 5.6 | Transformer components | 109 |
| 5.7 | Transformer | 110 |
| 5.8 | GPT model | 112 |
| 5.9 | ViT model | 114 |
| 6.1 | Convolutional object detector | 122 |
| 6.2 | Object detection with SSD | 123 |
| 6.3 | Semantic segmentation with PSP | 127 |
| 6.4 | CLIP zero-shot prediction | 133 |
| 6.5 | DQN state value evolution | 136 |
| 7.1 | Few-shot prediction with a GPT | 140 |
| 7.2 | Denoising diffusion | 143 |
| 8.1 | Chain-of-thought | 148 |
| 8.2 | Quantization | 151 |

Foreword

The current period of progress in artificial intelligence was triggered when Krizhevsky et al. [2012] demonstrated that an artificial neural network designed twenty years earlier [LeCun et al., 1989] could outperform complex state-of-the-art image recognition methods by a huge margin, simply by being a hundred times larger and trained on a dataset similarly scaled up.

This breakthrough was made possible thanks to Graphical Processing Units (GPUs), highly parallel consumer-grade computing devices developed for real-time image synthesis and repurposed for artificial neural networks.

Since then, under the umbrella term of “deep learning,” innovations in the structures of these networks, the strategies to train them, and dedicated hardware have allowed for an exponential increase in both their size and the quantity of training data they take advantage of [Sevilla

et al., 2022]. This has resulted in a wave of successful applications across technical domains, from computer vision and robotics to speech processing, and since 2020 in the development of Large Language Models with general proto-reasoning capabilities [Chowdhery et al., 2022].

Although the bulk of deep learning is not difficult to understand, it combines diverse components such as linear algebra, calculus, probabilities, optimization, signal processing, programming, algorithmics, and high-performance computing, making it complicated to learn.

Instead of trying to be exhaustive, this little book is limited to the background necessary to understand a few important models. This proved to be a popular approach, resulting in more than 500,000 downloads of the PDF file in the 12 months following its announcement on Twitter.

If you did not get this book from its official URL

<https://fleuret.org/public/lndl.pdf>

please do so, to allow the estimation of the number of readers.

François Fleuret,
May 19, 2024

PART I

FOUNDATIONS

Chapter 1

Machine Learning

Deep learning belongs historically to the larger field of statistical machine learning, as it fundamentally concerns methods that are able to learn representations from data. The techniques involved come originally from artificial neural networks, and the “deep” qualifier highlights that models are long compositions of mappings, now known to achieve greater performance.

The modularity, versatility, and scalability of deep models have resulted in a plethora of specific mathematical methods and software development tools, establishing deep learning as a distinct and vast technical field.

1.1 Learning from data

The simplest use case for a model trained from data is when a signal x is accessible, for instance, the picture of a license plate, from which one wants to predict a quantity y , such as the string of characters written on the plate.

In many real-world situations where x is a high-dimensional signal captured in an uncontrolled environment, it is too complicated to come up with an analytical recipe that relates x and y .

What one can do is to collect a large training set \mathcal{D} of pairs (x_n, y_n) , and devise a parametric model f . This is a piece of computer code that incorporates trainable parameters w that modulate its behavior, and such that, with the proper values w^* , it is a good predictor. “Good” here means that if an x is given to this piece of code, the value $\hat{y} = f(x; w^*)$ it computes is a good estimate of the y that would have been associated with x in the training set had it been there.

This notion of goodness is usually formalized with a loss $\mathcal{L}(w)$ which is small when $f(\cdot; w)$ is good on \mathcal{D} . Then, training the model consists of computing a value w^* that minimizes $\mathcal{L}(w^*)$.

Most of the content of this book is about the definition of f , which, in realistic scenarios, is a complex combination of pre-defined sub-modules.

The trainable parameters that compose w are often called weights, by analogy with the synaptic weights of biological neural networks. In addition to these parameters, models usually depend on hyper-parameters, which are set according to domain prior knowledge, best practices, or resource constraints. They may also be optimized in some way, but with techniques different from those used to optimize w .

1.2 Basis function regression

We can illustrate the training of a model in a simple case where x_n and y_n are two real numbers, the loss is the mean squared error:

$$\mathcal{L}(w) = \frac{1}{N} \sum_{n=1}^N (y_n - f(x_n; w))^2, \quad (1.1)$$

and $f(\cdot; w)$ is a linear combination of a pre-defined basis of functions f_1, \dots, f_K , with $w = (w_1, \dots, w_K)$:

$$f(x; w) = \sum_{k=1}^K w_k f_k(x).$$

Since $f(x_n; w)$ is linear with respect to the w_k s and $\mathcal{L}(w)$ is quadratic with respect to $f(x_n; w)$,

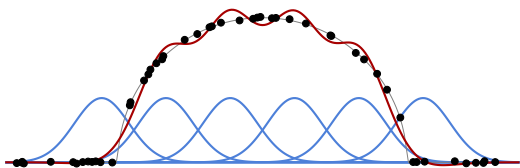


Figure 1.1: Given a basis of functions (blue curves) and a training set (black dots), we can compute an optimal linear combination of the former (red curve) to approximate the latter for the mean squared error.

the loss $\mathcal{L}(w)$ is quadratic with respect to the w_k s, and finding w^* that minimizes it boils down to solving a linear system. See Figure 1.1 for an example with Gaussian kernels as f_k .

1.3 Under and overfitting

A key element is the interplay between the capacity of the model, that is its flexibility and ability to fit diverse data, and the amount and quality of the training data. When the capacity is insufficient, the model cannot fit the data, resulting in a high error during training. This is referred to as underfitting.

On the contrary, when the amount of data is insufficient, as illustrated in Figure 1.2, the model will often learn characteristics specific to the training examples, resulting in excellent performance during training, at the cost of a worse

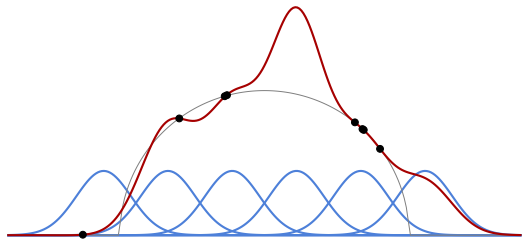


Figure 1.2: If the amount of training data (black dots) is small compared to the capacity of the model, the empirical performance of the fitted model during training (red curve) reflects poorly its actual fit to the underlying data structure (thin black curve), and consequently its usefulness for prediction.

fit to the global structure of the data, and poor performance on new inputs. This phenomenon is referred to as overfitting.

So, a large part of the art of applied machine learning is to design models that are not too flexible yet still able to fit the data. This is done by crafting the right inductive bias in a model, which means that its structure corresponds to the underlying structure of the data at hand.

Even though this classical perspective is relevant for reasonably-sized deep models, things get confusing with large ones that have a very large number of trainable parameters and extreme capacity yet still perform well on prediction. We will come back to this in § 3.6 and § 3.7.

1.4 Categories of models

We can organize the use of machine learning models into three broad categories:

- Regression consists of predicting a continuous-valued vector $y \in \mathbb{R}^K$, for instance, a geometrical position of an object, given an input signal X . This is a multi-dimensional generalization of the setup we saw in § 1.2. The training set is composed of pairs of an input signal and a ground-truth value.
- Classification aims at predicting a value from a finite set $\{1, \dots, C\}$, for instance, the label Y of an image X . As with regression, the training set is composed of pairs of input signal, and ground-truth quantity, here a label from that set. The standard way of tackling this is to predict one score per potential class, such that the correct class has the maximum score.
- Density modeling has as its objective to model the probability density function of the data μ_X itself, for instance, images. In that case, the training set is composed of values x_n without associated quantities to predict, and the trained model should allow for the evaluation of the probability density function, or sampling from the distribution, or both.

Both regression and classification are generally referred to as supervised learning, since the value to be predicted, which is required as a target during training, has to be provided, for instance, by human experts. On the contrary, density modeling is usually seen as unsupervised learning, since it is sufficient to take existing data without the need for producing an associated ground-truth.

These three categories are not disjoint; for instance, classification can be cast as class-score regression, or discrete sequence density modeling as iterated classification. Furthermore, they do not cover all cases. One may want to predict compounded quantities, or multiple classes, or model a density conditional on a signal.

Chapter 2

Efficient Computation

From an implementation standpoint, deep learning is about executing heavy computations with large amounts of data. The Graphical Processing Units (GPUs) have been instrumental in the success of the field by allowing such computations to be run on affordable hardware.

The importance of their use, and the resulting technical constraints on the computations that can be done efficiently, force the research in the field to constantly balance mathematical soundness and implementability of novel methods.

2.1 *GPUs, TPUs, and batches*

Graphical Processing Units were originally designed for real-time image synthesis, which requires highly parallel architectures that happen to be well suited for deep models. As their usage for AI has increased, GPUs have been equipped with dedicated tensor cores, and deep-learning specialized chips such as Google's Tensor Processing Units (TPUs) have been developed.

A GPU possesses several thousand parallel units and its own fast memory. The limiting factor is usually not the number of computing units, but the read-write operations to memory. The slowest link is between the CPU memory and the GPU memory, and consequently one should avoid copying data across devices. Moreover, the structure of the GPU itself involves multiple levels of cache memory, which are smaller but faster, and computation should be organized to avoid copies between these different caches.

This is achieved, in particular, by organizing the computation in batches of samples that can fit entirely in the GPU memory and are processed in parallel. When an operator combines a sample and model parameters, both have to be moved to the cache memory near the actual computing

units. Proceeding by batches allows for copying the model parameters only once, instead of doing it for each sample. In practice, a GPU processes a batch that fits in memory almost as quickly as it would process a single sample.

A standard GPU has a theoretical peak performance of 10^{13} – 10^{14} floating-point operations (FLOPs) per second, and its memory typically ranges from 8 to 80 gigabytes. The standard FP32 encoding of float numbers is on 32 bits, but empirical results show that using encoding on 16 bits, or even less for some operands, does not degrade performance.

We will come back in § 3.7 to the large size of deep architectures.

2.2 Tensors

GPUs and deep learning frameworks such as PyTorch or JAX manipulate the quantities to be processed by organizing them as tensors, which are series of scalars arranged along several discrete axes. They are elements of $\mathbb{R}^{N_1 \times \dots \times N_D}$ that generalize the notion of vector and matrix.

Tensors are used to represent both the signals to be processed, the trainable parameters of the models, and the intermediate quantities they compute. The latter are called activations, in reference to neuronal activations.

For instance, a time series is naturally encoded as a $T \times D$ tensor, or, for historical reasons, as a $D \times T$ tensor, where T is its duration and D is the dimension of the feature representation at every time step, often referred to as the number of channels. Similarly, a 2D-structured signal can be represented as a $D \times H \times W$ tensor, where H and W are its height and width. An RGB image would correspond to $D = 3$, but the number of channels can grow up to several thousands in large models.

Adding more dimensions allows for the representation of series of objects. For example, fifty RGB images of resolution 32×24 can be encoded as

a $50 \times 3 \times 24 \times 32$ tensor.

Deep learning libraries provide a large number of operations that encompass standard linear algebra, complex reshaping and extraction, and deep-learning specific operations, some of which we will see in Chapter 4. The implementation of tensors separates the shape representation from the storage layout of the coefficients in memory, which allows many reshaping, transposing, and extraction operations to be done without coefficient copying, hence extremely rapidly.

In practice, virtually any computation can be decomposed into elementary tensor operations, which avoids non-parallel loops at the language level and poor memory management.

Besides being convenient tools, tensors are instrumental in achieving computational efficiency. All the people involved in the development of an operational deep model, from the designers of the drivers, libraries, and models to those of the computers and chips, know that the data will be manipulated as tensors. The resulting constraints on locality and block decomposability enable all the actors in this chain to come up with optimal designs.

Chapter 3

Training

As introduced in § 1.1, training a model consists of minimizing a loss $\mathcal{L}(w)$ which reflects the performance of the predictor $f(\cdot; w)$ on a training set \mathcal{D} .

Since models are usually extremely complex, and their performance is directly related to how well the loss is minimized, this minimization is a key challenge, which involves both computational and mathematical difficulties.

3.1 Losses

The example of the mean squared error from Equation 1.1 is a standard loss for predicting a continuous value.

For density modeling, the standard loss is the likelihood of the data. If $f(x; w)$ is to be interpreted as a normalized log-probability or log-density, the loss is the opposite of the sum of its values over training samples, which corresponds to the likelihood of the data-set.

Cross-entropy

For classification, the usual strategy is that the output of the model is a vector with one component $f(x; w)_y$ per class y , interpreted as the logarithm of a non-normalized probability, or logit.

With X the input signal and Y the class to predict, we can then compute from f an estimate of the posterior probabilities:

$$\hat{P}(Y = y \mid X = x) = \frac{\exp f(x; w)_y}{\sum_z \exp f(x; w)_z}.$$

This expression is generally called the softmax, or more adequately, the softargmax, of the logits.

To be consistent with this interpretation, the model should be trained to maximize the probability of the true classes, hence to minimize the cross-entropy, expressed as:

$$\begin{aligned}\mathcal{L}_{\text{ce}}(w) &= -\frac{1}{N} \sum_{n=1}^N \log \hat{P}(Y = y_n \mid X = x_n) \\ &= \frac{1}{N} \sum_{n=1}^N \underbrace{-\log \frac{\exp f(x_n; w)_{y_n}}{\sum_z \exp f(x_n; w)_z}}_{L_{\text{ce}}(f(x_n; w), y_n)}.\end{aligned}$$

Contrastive loss

In certain setups, even though the value to be predicted is continuous, the supervision takes the form of ranking constraints. The typical domain where this is the case is metric learning, where the objective is to learn a measure of distance between samples such that a sample x_a from a certain semantic class is closer to any sample x_b of the same class than to any sample x_c from another class. For instance, x_a and x_b can be two pictures of a certain person, and x_c a picture of someone else.

The standard approach for such cases is to minimize a contrastive loss, in that case, for instance, the sum over triplets (x_a, x_b, x_c) , such

that $y_a = y_b \neq y_c$, of

$$\max(0, 1 - f(x_a, x_c; w) + f(x_a, x_b; w)).$$

This quantity will be strictly positive unless $f(x_a, x_c; w) \geq 1 + f(x_a, x_b; w)$.

Engineering the loss

Usually, the loss minimized during training is not the actual quantity one wants to optimize ultimately, but a proxy for which finding the best model parameters is easier. For instance, cross-entropy is the standard loss for classification, even though the actual performance measure is a classification error rate, because the latter has no informative gradient, a key requirement as we will see in § 3.3.

It is also possible to add terms to the loss that depend on the trainable parameters of the model themselves to favor certain configurations.

The weight decay regularization, for instance, consists of adding to the loss a term proportional to the sum of the squared parameters. This can be interpreted as having a Gaussian Bayesian prior on the parameters, which favors smaller values and thereby reduces the influence of the data. This degrades performance on the train-

ing set, but reduces the gap between the performance in training and that on new, unseen data.

3.2 Autoregressive models

A key class of methods, particularly for dealing with discrete sequences in natural language processing and computer vision, are the autoregressive models,

The chain rule for probabilities

Such models put to use the chain rule from probability theory:

$$\begin{aligned} P(X_1 = x_1, X_2 = x_2, \dots, X_T = x_T) &= \\ P(X_1 = x_1) & \\ \times P(X_2 = x_2 | X_1 = x_1) & \\ \dots & \\ \times P(X_T = x_T | X_1 = x_1, \dots, X_{T-1} = x_{T-1}). & \end{aligned}$$

Although this decomposition is valid for a random sequence of any type, it is particularly efficient when the signal of interest is a sequence of tokens from a finite vocabulary $\{1, \dots, K\}$.

With the convention that the additional token \emptyset stands for an “unknown” quantity, we can represent the event $\{X_1 = x_1, \dots, X_t = x_t\}$ as the vector $(x_1, \dots, x_t, \emptyset, \dots, \emptyset)$.

Then, a model

$$f : \{\emptyset, 1, \dots, K\}^T \rightarrow \mathbb{R}^K$$

which, given such an input, computes a vector l_t of K logits corresponding to

$$\hat{P}(X_t | X_1 = x_1, \dots, X_{t-1} = x_{t-1}),$$

allows to sample one token given the previous ones.

The chain rule ensures that by sampling T tokens x_t , one at a time given the previously sampled x_1, \dots, x_{t-1} , we get a sequence that follows the joint distribution. This is an autoregressive generative model.

Training such a model can be done by minimizing the sum across training sequences and time steps of the cross-entropy loss

$$L_{\text{ce}}(f(x_1, \dots, x_{t-1}, \emptyset, \dots, \emptyset; w), x_t),$$

which is formally equivalent to maximizing the likelihood of the true x_t s.

The value that is classically monitored is not the cross-entropy itself, but the perplexity, which is defined as the exponential of the cross-entropy. It corresponds to the number of values of a uniform distribution with the same entropy, which is generally more interpretable.

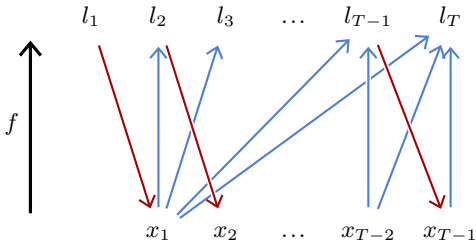


Figure 3.1: An autoregressive model f , is causal if a time step x_t of the input sequence modulates the predicted logits l_s only if $s > t$, as depicted by the blue arrows. This allows computing the distributions at all the time steps in one pass during training. During sampling, however, the l_t and x_t are computed sequentially, the latter sampled with the former, as depicted by the red arrows.

Causal models

The training procedure we just described requires a different input for each t , and the bulk of the computation done for $t < t'$ is repeated for t' . This is extremely inefficient since T is often of the order of hundreds or thousands.

The standard strategy to address this issue is to design a model f that predicts all the vectors of logits l_1, \dots, l_T at once, that is:

$$f : \{1, \dots, K\}^T \rightarrow \mathbb{R}^{T \times K},$$

but with a computational structure such that the computed logits l_t for x_t depend only on the input values x_1, \dots, x_{t-1} .

Such a model is called causal, since it corresponds, in the case of temporal series, to not letting the future influence the past, as illustrated in Figure 3.1.

The consequence is that the output at every position is the one that would be obtained if the input were only available up to before that position. During training, it allows one to compute the output for a full sequence and to maximize the predicted probabilities of all the tokens of that same sequence, which again boils down to minimizing the sum of the per-token cross-entropy.

Note that, for the sake of simplicity, we have defined f as operating on sequences of a fixed length T . However, models used in practice, such as the transformers we will see in § 5.3, are able to process sequences of arbitrary length.

Tokenizer

One important technical detail when dealing with natural languages is that the representation as tokens can be done in multiple ways, ranging from the finest granularity of individual symbols

to entire words. The conversion to and from the token representation is carried out by a separate algorithm called a tokenizer.

A standard method is the Byte Pair Encoding (BPE) [[Sennrich et al., 2015](#)] that constructs tokens by hierarchically merging groups of characters, trying to get tokens that represent fragments of words of various lengths but of similar frequencies, allocating tokens to long frequent fragments as well as to rare individual symbols.

3.3 Gradient descent

Except in specific cases like the linear regression we saw in § 1.2, the optimal parameters w^* do not have a closed-form expression. In the general case, the tool of choice to minimize a function is gradient descent. It starts by initializing the parameters with a random w_0 , and then improves this estimate by iterating gradient steps, each consisting of computing the gradient of the loss with respect to the parameters, and subtracting a fraction of it:

$$w_{n+1} = w_n - \eta \nabla \mathcal{L}|_w(w_n). \quad (3.1)$$

This procedure corresponds to moving the current estimate a bit in the direction that locally decreases $\mathcal{L}(w)$ maximally, as illustrated in Figure 3.2.

Learning rate

The hyper-parameter η is called the learning rate. It is a positive value that modulates how quickly the minimization is done, and must be chosen carefully.

If it is too small, the optimization will be slow at best, and may be trapped in a local minimum early. If it is too large, the optimization may

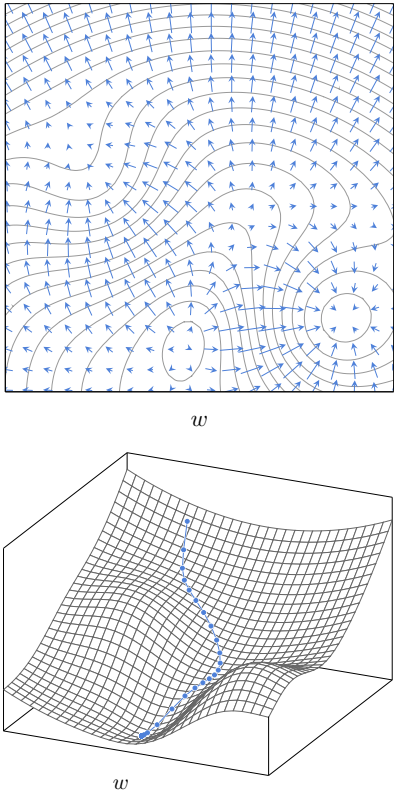


Figure 3.2: At every point w , the gradient $\nabla \mathcal{L}|_w(w)$ is in the direction that maximizes the increase of \mathcal{L} , orthogonal to the level curves (top). The gradient descent minimizes $\mathcal{L}(w)$ iteratively by subtracting a fraction of the gradient at every step, resulting in a trajectory that follows the steepest descent (bottom).

bounce around a good minimum and never descend into it. As we will see in § 3.6, it can depend on the iteration number n .

Stochastic Gradient Descent

All the losses used in practice can be expressed as an average of a loss per small group of samples, or per sample such as:

$$\mathcal{L}(w) = \frac{1}{N} \sum_{n=1}^N \ell_n(w),$$

where $\ell_n(w) = L(f(x_n; w), y_n)$ for some L , and the gradient is then:

$$\nabla \mathcal{L}|_w(w) = \frac{1}{N} \sum_{n=1}^N \nabla \ell_n|_w(w). \quad (3.2)$$

The resulting gradient descent would compute exactly the sum in Equation 3.2, which is usually computationally heavy, and then update the parameters according to Equation 3.1. However, under reasonable assumptions of exchangeability, for instance, if the samples have been properly shuffled, any partial sum of Equation 3.2 is an unbiased estimator of the full sum, albeit noisy. So, updating the parameters from partial sums corresponds to doing more gradient steps

for the same computational budget, with noisier estimates of the gradient. Due to the redundancy in the data, this happens to be a far more efficient strategy.

We saw in § 2.1 that processing a batch of samples small enough to fit in the computing device’s memory is generally as fast as processing a single one. Hence, the standard approach is to split the full set \mathcal{D} into batches, and to update the parameters from the estimate of the gradient computed from each. This is called mini-batch stochastic gradient descent, or stochastic gradient descent (SGD) for short.

It is important to note that this process is extremely gradual, and that the number of mini-batches and gradient steps are typically of the order of several million.

As with many algorithms, intuition breaks down in high dimensions, and although it may seem that this procedure would be easily trapped in a local minimum, in reality, due to the number of parameters, the design of the models, and the stochasticity of the data, its efficiency is far greater than one might expect.

Plenty of variations of this standard strategy have been proposed. The most popular one is

Adam [Kingma and Ba, 2014], which keeps running estimates of the mean and variance of each component of the gradient, and normalizes them automatically, avoiding scaling issues and different training speeds in different parts of a model.

3.4 Backpropagation

Using gradient descent requires a technical means to compute $\nabla \ell|_w(w)$ where $\ell = L(f(x; w); y)$. Given that f and L are both compositions of standard tensor operations, as for any mathematical expression, the chain rule from differential calculus allows us to get an expression of it.

For the sake of making notation lighter, we will not specify at which point gradients are computed, since the context makes it clear.

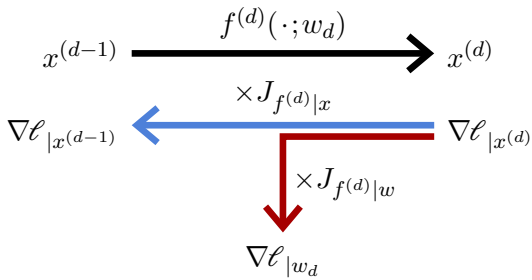


Figure 3.3: Given a model $f = f^{(D)} \circ \dots \circ f^{(1)}$, the forward pass computes the outputs $x^{(d)}$ of the $f^{(d)}$ in order (top, black). The backward pass computes the gradients of the loss with respect to the activations $x^{(d)}$ (bottom, blue) and the parameters w_d (bottom, red) backward by multiplying them by the Jacobians.

Forward and backward passes

Consider the simple case of a composition of mappings:

$$f = f^{(D)} \circ f^{(D-1)} \circ \dots \circ f^{(1)}.$$

The output of $f(x; w)$ can be computed by starting with $x^{(0)} = x$ and applying iteratively:

$$x^{(d)} = f^{(d)}\left(x^{(d-1)}; w_d\right),$$

with $x^{(D)}$ as the final value.

The individual scalar values of these intermediate results $x^{(d)}$ are traditionally called activations in reference to neuron activations, the value D is the depth of the model, the individual mappings $f^{(d)}$ are referred to as layers, as we will see in § 4.1, and their sequential evaluation is the forward pass (see Figure 3.3, top).

Conversely, the gradient $\nabla \ell|_{x^{(d-1)}}$ of the loss with respect to the output $x^{(d-1)}$ of $f^{(d-1)}$ is the product of the gradient $\nabla \ell|_{x^{(d)}}$ with respect to the output of $f^{(d)}$ multiplied by the Jacobian $J_{f^{(d-1)}|x}$ of $f^{(d-1)}$ with respect to its variable x . Thus, the gradients with respect to the outputs of all the $f^{(d)}$ s can be computed recursively backward, starting with $\nabla \ell|_{x^{(D)}} = \nabla L|_x$.

And the gradient that we are interested in for training, that is $\nabla \ell|_{w_d}$, is the gradient with respect to the output of $f^{(d)}$ multiplied by the Jacobian $J_{f^{(d)}|_w}$ of $f^{(d)}$ with respect to the parameters.

This iterative computation of the gradients with respect to the intermediate activations, combined with that of the gradients with respect to the layers' parameters, is the backward pass (see Figure 3.3, bottom). The combination of this computation with the procedure of gradient descent is called backpropagation.

In practice, the implementation details of the forward and backward passes are hidden from programmers. Deep learning frameworks are able to automatically construct the sequence of operations to compute gradients.

A particularly convenient algorithm is Autograd [Baydin et al., 2015], which tracks tensor operations and builds, on the fly, the combination of operators for gradients. Thanks to this, a piece of imperative programming that manipulates tensors can automatically compute the gradient of any quantity with respect to any other.

Resource usage

Regarding the computational cost, as we will see, the bulk of the computation goes into linear operations, each requiring one matrix product for the forward pass and two for the products by the Jacobians for the backward pass, making the latter roughly twice as costly as the former.

The memory requirement during inference is roughly equal to that of the most demanding individual layer. For training, however, the backward pass requires keeping the activations computed during the forward pass to compute the Jacobians, which results in a memory usage that grows proportionally to the model's depth. Techniques exist to trade the memory usage for computation by either relying on reversible layers [[Gomez et al., 2017](#)], or using checkpointing, which consists of storing activations for some layers only and recomputing the others on the fly with partial forward passes during the backward pass [[Chen et al., 2016](#)].

Vanishing gradient

A key historical issue when training a large network is that when the gradient propagates backwards through an operator, it may be scaled by a

multiplicative factor, and consequently decrease or increase exponentially when it traverses many layers. A standard method to prevent it from exploding is gradient norm clipping, which consists of re-scaling the gradient to set its norm to a fixed threshold if it is above it [[Pascanu et al., 2013](#)].

When the gradient decreases exponentially, this is called the vanishing gradient, and it may make the training impossible, or, in its milder form, cause different parts of the model to be updated at different speeds, degrading their co-adaptation [[Glorot and Bengio, 2010](#)].

As we will see in Chapter 4, multiple techniques have been developed to prevent this from happening, reflecting a change in perspective that was crucial to the success of deep-learning: instead of trying to improve generic optimization methods, the effort shifted to engineering the models themselves to make them optimizable.

3.5 *The value of depth*

As the term “deep learning” indicates, useful models are generally compositions of long series of mappings. Training them with gradient descent results in a sophisticated co-adaptation of the mappings, even though this procedure is gradual and local.

We can illustrate this behavior with a simple model $\mathbb{R}^2 \rightarrow \mathbb{R}^2$ that combines eight layers, each multiplying its input by a 2×2 matrix and applying Tanh per component, with a final linear classifier. This is a simplified version of the standard Multi-Layer Perceptron that we will see in § 5.1.

If we train this model with SGD and cross-entropy on a toy binary classification task (Figure 3.4, top left), the matrices co-adapt to deform the space until the classification is correct, which implies that the data have been made linearly separable before the final affine operation (Figure 3.4, bottom right).

Such an example gives a glimpse of what a deep model can achieve; however, it is partially misleading due to the low dimension of both the signal to process and the internal representations. Everything is kept in 2D here for the sake of

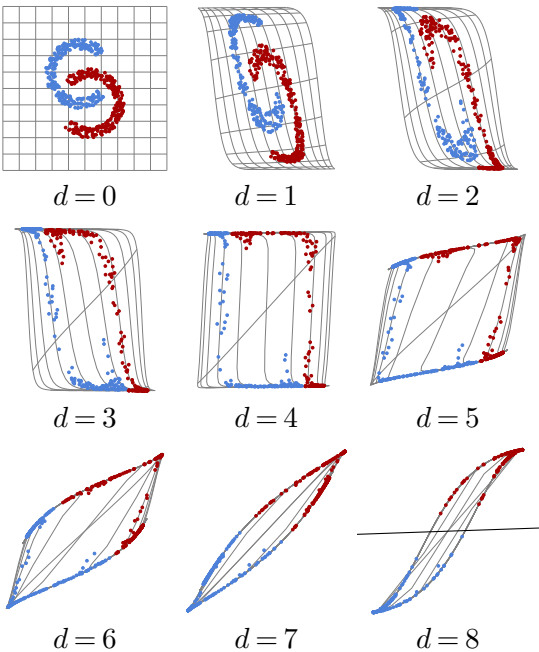


Figure 3.4: Each plot shows the deformation of the space and the resulting positioning of the training points in \mathbb{R}^2 after d layers of processing, starting with the input to the model itself (top left). The oblique line in the last plot (bottom right) shows the final affine decision.

visualization, while real models take advantage of representations in high dimensions, which, in particular, facilitates the optimization by providing many degrees of freedom.

Empirical evidence accumulated over twenty years demonstrates that state-of-the-art performance across application domains necessitates models with tens of layers, such as residual networks (see § 5.2) or Transformers (see § 5.3).

Theoretical results show that, for a fixed computational budget or number of parameters, increasing the depth leads to a greater complexity of the resulting mapping [Telgarsky, 2016].

3.6 *Training protocols*

Training a deep network requires defining a protocol to make the most of computation and data, and to ensure that performance will be good on new data.

As we saw in § 1.3, the performance on the training samples may be misleading, so in the simplest setup one needs at least two sets of samples: one is a training set, used to optimize the model parameters, and the other is a test set, to evaluate the performance of the trained model.

Additionally, there are usually hyper-parameters to adapt, in particular, those related to the model architecture, the learning rate, and the regularization terms in the loss. In that case, one needs a validation set that is disjoint from both the training and test sets to assess the best configuration.

The full training is usually decomposed into epochs, each of which corresponds to going through all the training examples once. The usual dynamic of the losses is that the training loss decreases as long as the optimization runs, while the validation loss may reach a minimum after a certain number of epochs and then start to increase, reflecting an overfitting regime, as

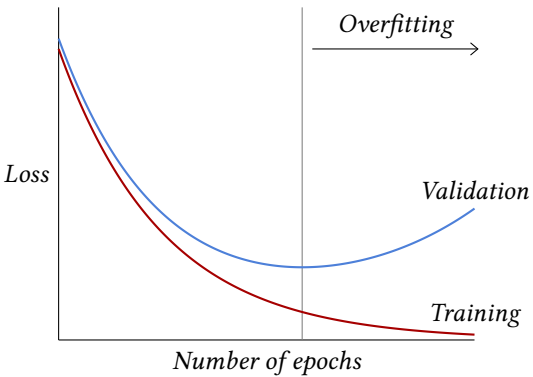


Figure 3.5: As training progresses, a model's performance is usually monitored through losses. The training loss is the one driving the optimization process and goes down, while the validation loss is estimated on an other set of examples to assess the overfitting of the model. Overfitting appears when the model starts to take into account random structures specific to the training set at hand, resulting in the validation loss starting to increase.

introduced in § 1.3 and illustrated in Figure 3.5.

Paradoxically, although they should suffer from severe overfitting due to their capacity, large models usually continue to improve as training progresses. This may be due to the inductive bias of the model becoming the main driver of optimization when performance is near perfect

on the training set [Belkin et al., 2018].

An important design choice is the learning rate schedule during training, that is, the specification of the value of the learning rate at each iteration of the gradient descent. The general policy is that the learning rate should be initially large to avoid having the optimization being trapped in a bad local minimum early, and that it should get smaller so that the optimized parameter values do not bounce around and reach a good minimum in a narrow valley of the loss landscape.

The training of very large models may take months on thousands of powerful GPUs and have a financial cost of several million dollars. At this scale, the training may involve many manual interventions, informed, in particular, by the dynamics of the loss evolution.

Fine-tuning

It is often beneficial to adapt an already trained model to a new task, referred to as a downstream task.

It can be because the amount of data for the original task is plentiful, while they are limited for the downstream task, and the two tasks share enough similarities that statistical struc-

tures learned for the first provide a good inductive bias for the second. It can also be to limit the training cost by reusing the patterns encoded in an existing model.

Adapting a pre-trained model to a specific task is achieved with fine-tuning, which is a standard training procedure for the downstream task, but which starts from the pre-trained model instead of using a random initialization.

This is the main strategy for most computer vision applications which generally use a model pre-trained for classification on ImageNet [Deng et al., 2009] (see § 6.3 and § 6.4), and it is also how purely generative pre-trained Large Language Models are re-purposed as assistant-like models, able to produce interactive dialogues (see § 7.1).

We come back to techniques to cope with limited resources in inference and for fine-tuning in Chapter 8.

3.7 *The benefits of scale*

There is an accumulation of empirical results showing that performance, for instance, estimated through the loss on test data, improves with the amount of data according to remarkable scaling laws, as long as the model size increases correspondingly [Kaplan et al., 2020] (see Figure 3.6).

Benefiting from these scaling laws in the multi-billion sample regime is possible in part thanks to the structure of deep models which can be scaled up arbitrarily, as we will see, by increasing the number of layers or feature dimensions. But it is also made possible by the distributed nature of the computation they implement, and by the stochastic gradient descent, which requires only a fraction of the data at a time and can operate with datasets whose size is orders of magnitude greater than that of the computing device's memory. This has resulted in an exponential growth of the models, as illustrated in Figure 3.7.

Typical vision models have 10–100 million trainable parameters and require 10^{18} – 10^{19} FLOPs for training [He et al., 2015; Sevilla et al., 2022]. Language models have from 100 million to hundreds of billions of trainable parameters and re-

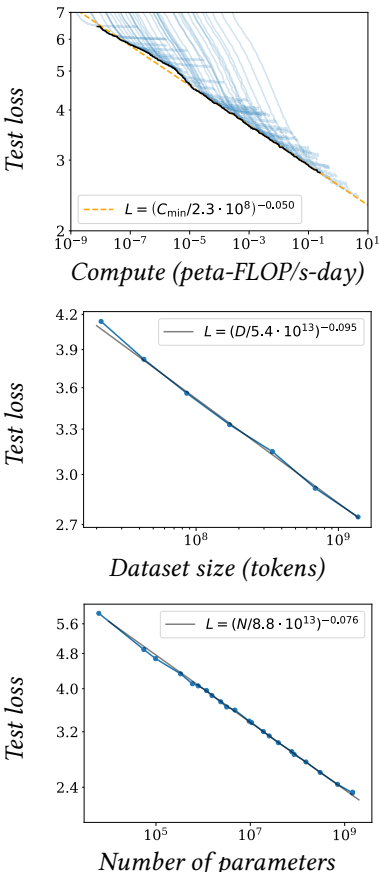


Figure 3.6: *Test loss of a language model vs. the amount of computation in petaflop/s-day, the dataset size in tokens, that is fragments of words, and the model size in parameters [Kaplan et al., 2020].*

| Dataset | Year | Nb. of images | Size |
|----------------|-------------|----------------------|-------------|
| ImageNet | 2012 | 1.2M | 150Gb |
| Cityscape | 2016 | 25K | 60Gb |
| LAION-5B | 2022 | 5.8B | 240Tb |
| Dataset | Year | Nb. of books | Size |
| WMT-18-de-en | 2018 | 14M | 8Gb |
| The Pile | 2020 | 1.6B | 825Gb |
| OSCAR | 2020 | 12B | 6Tb |

Table 3.1: *Some examples of publicly available datasets. The equivalent number of books is an indicative estimate for 250 pages of 2000 characters per book.*

quire 10^{20} – 10^{23} FLOPs for training [Devlin et al., 2018; Brown et al., 2020; Chowdhery et al., 2022; Sevilla et al., 2022]. These latter models require machines with multiple high-end GPUs.

Training these large models is impossible using datasets with a detailed ground-truth costly to produce, which can only be of moderate size. Instead, it is done with datasets automatically produced by combining data available on the internet with minimal curation, if any. These sets may combine multiple modalities, such as text and images from web pages, or sound and images from videos, which can be used for large-scale supervised training.

As of 2024, the most powerful models are the

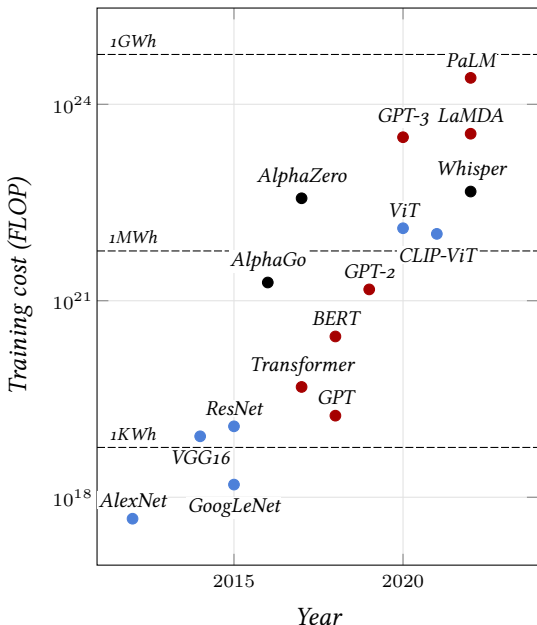


Figure 3.7: *Training costs in number of FLOP of some landmark models [Sevilla et al., 2023]. The colors indicate the domains of application: Computer Vision (blue), Natural Language Processing (red), or other (black). The dashed lines correspond to the energy consumption using A100s SXM in 16-bit precision. For reference, the total electricity consumption in the US in 2021 was 3920 TWh.*

so-called Large Language Models (LLMs), which we will see in § 5.3 and § 7.1, trained on extremely large text datasets (see Table 3.1).

PART II

DEEP MODELS

Chapter 4

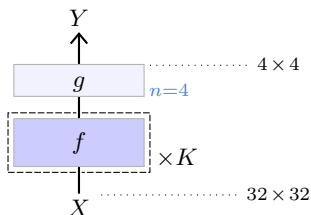
Model Components

A deep model is nothing more than a complex tensorial computation that can ultimately be decomposed into standard mathematical operations from linear algebra and analysis. Over the years, the field has developed a large collection of high-level modules with a clear semantic, and complex models combining these modules, which have proven to be effective in specific application domains.

Empirical evidence and theoretical results show that greater performance is achieved with deeper architectures, that is, long compositions of mappings. As we saw in section § 3.4, training such a model is challenging due to the vanishing gradient, and multiple important technical contributions have mitigated this issue.

4.1 The notion of layer

We call layers standard complex compounded tensor operations that have been designed and empirically identified as being generic and efficient. They often incorporate trainable parameters and correspond to a convenient level of granularity for designing and describing large deep models. The term is inherited from simple multi-layer neural networks, even though modern models may take the form of a complex graph of such modules, incorporating multiple parallel pathways.



In the following pages, I try to stick to the convention for model depiction illustrated above:

- operators / layers are depicted as boxes,
- darker coloring indicates that they embed trainable parameters,
- non-default valued hyper-parameters are

added in blue on their right,

- a dashed outer frame with a multiplicative factor indicates that a group of layers is replicated in series, each with its own set of trainable parameters, if any, and
- in some cases, the dimension of their output is specified on the right when it differs from their input.

Additionally, layers that have a complex internal structure are depicted with a greater height.

4.2 Linear layers

The most important modules in terms of computation and number of parameters are the Linear layers. They benefit from decades of research and engineering in algorithmic and chip design for matrix operations.

Note that the term “linear” in deep learning generally refers improperly to an affine operation, which is the sum of a linear expression and a constant bias.

Fully connected layers

The most basic linear layer is the fully connected layer, parameterized by a trainable weight matrix W of size $D' \times D$ and bias vector b of dimension D' . It implements an affine transformation generalized to arbitrary tensor shapes, where the supplementary dimensions are interpreted as vector indexes. Formally, given an input X of dimension $D_1 \times \dots \times D_K \times D$, it computes an output Y of dimension $D_1 \times \dots \times D_K \times D'$ with

$$\forall d_1, \dots, d_K,$$

$$Y[d_1, \dots, d_K] = W X[d_1, \dots, d_K] + b.$$

While at first sight such an affine operation

seems limited to geometric transformations such as rotations, symmetries, and translations, it can in fact do more than that. In particular, projections for dimension reduction or signal filtering, but also, from the perspective of the dot product being a measure of similarity, a matrix-vector product can be interpreted as computing matching scores between the queries, as encoded by the input vectors, and keys, as encoded by the matrix rows.

As we saw in § 3.3, the gradient descent starts with the parameters' random initialization. If this is done too naively, as seen in § 3.4, the network may suffer from exploding or vanishing activations and gradients [Glorot and Bengio, 2010]. Deep learning frameworks implement initialization methods that in particular scale the random parameters according to the dimension of the input to keep the variance of the activations constant and prevent pathological behaviors.

Convolutional layers

A linear layer can take as input an arbitrarily-shaped tensor by reshaping it into a vector, as long as it has the correct number of coefficients. However, such a layer is poorly adapted to deal-

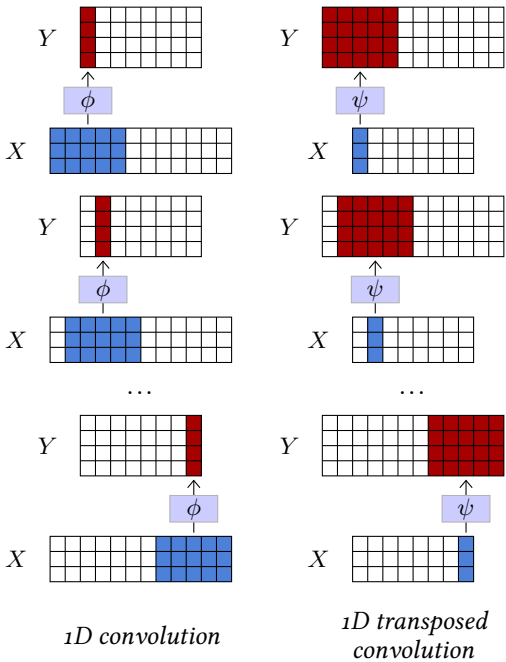


Figure 4.1: A 1D convolution (left) takes as input a $D \times T$ tensor X , applies the same affine mapping $\phi(\cdot; w)$ to every sub-tensor of shape $D \times K$, and stores the resulting $D' \times 1$ tensors into Y . A 1D transposed convolution (right) takes as input a $D \times T$ tensor, applies the same affine mapping $\psi(\cdot; w)$ to every sub-tensor of shape $D \times 1$, and sums the shifted resulting $D' \times K$ tensors. Both can process inputs of different sizes.

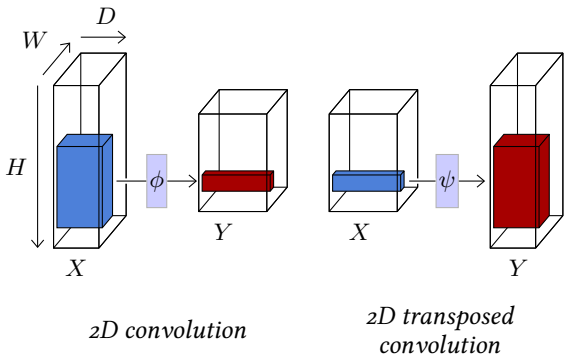


Figure 4.2: A 2D convolution (left) takes as input a $D \times H \times W$ tensor X , applies the same affine mapping $\phi(\cdot; w)$ to every sub-tensor of shape $D \times K \times L$, and stores the resulting $D' \times 1 \times 1$ tensors into Y . A 2D transposed convolution (right) takes as input a $D \times H \times W$ tensor, applies the same affine mapping $\psi(\cdot; w)$ to every $D \times 1 \times 1$ sub-tensor, and sums the shifted resulting $D' \times K \times L$ tensors into Y .

ing with large tensors, since the number of parameters and number of operations are proportional to the product of the input and output dimensions. For instance, to process an RGB image of size 256×256 as input and compute a result of the same size, it would require approximately 4×10^{10} parameters and multiplications.

Besides these practical issues, most of the high-dimension signals are strongly structured. For

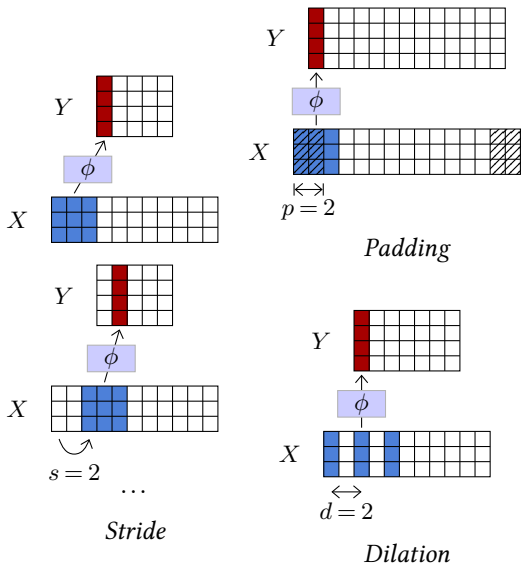


Figure 4.3: Beside its kernel size and number of input / output channels, a convolution admits three hyperparameters: the stride s (left) modulates the step size when going through the input tensor, the padding p (top right) specifies how many zero entries are added around the input tensor before processing it, and the dilation d (bottom right) parameterizes the index count between coefficients of the filter.

instance, images exhibit short-term correlations and statistical stationarity with respect to translation, scaling, and certain symmetries. This is not reflected in the inductive bias of a fully connected layer, which completely ignores the signal structure.

To leverage these regularities, the tool of choice is convolutional layers, which are also affine, but process time-series or 2D signals locally, with the same operator everywhere.

A 1D convolution is mainly defined by three hyper-parameters: its kernel size K , its number of input channels D , its number of output channels D' , and by the trainable parameters w of an affine mapping $\phi(\cdot; w) : \mathbb{R}^{D \times K} \rightarrow \mathbb{R}^{D' \times 1}$.

It can process any tensor X of size $D \times T$ with $T \geq K$, and applies $\phi(\cdot; w)$ to every sub-tensor of size $D \times K$ of X , storing the results in a tensor Y of size $D' \times (T - K + 1)$, as pictured in Figure 4.1 (left).

A 2D convolution is similar but has a $K \times L$ kernel and takes as input a $D \times H \times W$ tensor (see Figure 4.2, left).

Both operators have for trainable parameters those of ϕ that can be envisioned as D' filters

of size $D \times K$ or $D \times K \times L$ respectively, and a bias vector of dimension D' .

Such a layer is equivariant to translation, meaning that if the input signal is translated, the output is similarly transformed. This property results in a desirable inductive bias when dealing with a signal whose distribution is invariant to translation.

They also admit three additional hyper-parameters, illustrated on Figure 4.3:

- The padding specifies how many zero coefficients should be added around the input tensor before processing it, particularly to maintain the tensor size when the kernel size is greater than one. Its default value is 0.
- The stride specifies the step size used when going through the input, allowing one to reduce the output size geometrically by using large steps. Its default value is 1.
- The dilation specifies the index count between the filter coefficients of the local affine operator. Its default value is 1, and greater values correspond to inserting zeros between the coefficients, which increases the filter / kernel size while keeping the number of trainable parameters the same.

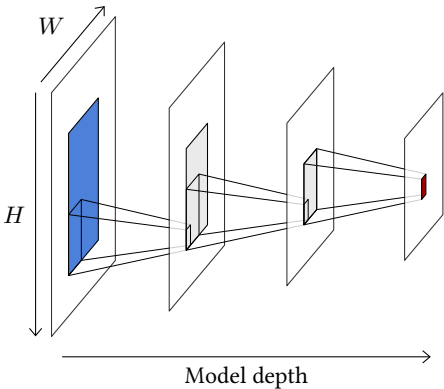


Figure 4.4: Given an activation in a series of convolution layers, here in red, its receptive field is the area in the input signal, in blue, that modulates its value. Each intermediate convolutional layer increases the width and height of that area by roughly those of the kernel.

ters unchanged.

Except for the number of channels, a convolution’s output is usually smaller than its input. In the 1D case without padding nor dilation, if the input is of size T , the kernel of size K , and the stride is S , the output is of size $T' = (T - K)/S + 1$.

Given an activation computed by a convolutional layer, or the vector of values for all the channels at a certain location, the portion of the input

signal that it depends on is called its receptive field (see Figure 4.4). One of the $H \times W$ sub-tensors corresponding to a single channel of a $D \times H \times W$ activation tensor is called an activation map.

Convolutions are used to recombine information, generally to reduce the spatial size of the representation, in exchange for a greater number of channels, which translates into a richer local representation. They can implement differential operators such as edge-detectors, or template matching mechanisms. A succession of such layers can also be envisioned as a compositional and hierarchical representation [Zeiler and Fergus, 2014], or as a diffusion process in which information can be transported by half the kernel size when passing through a layer.

A converse operation is the transposed convolution that also consists of a localized affine operator, defined by similar hyper and trainable parameters as the convolution, but which, for instance, in the 1D case, applies an affine mapping $\psi(\cdot; w) : \mathbb{R}^{D \times 1} \rightarrow \mathbb{R}^{D' \times K}$, to every $D \times 1$ sub-tensor of the input, and sums the shifted $D' \times K$ resulting tensors to compute its output. Such an operator increases the size of the signal and can be understood intuitively as a synthe-

sis process (see Figure 4.1, right, and Figure 4.2, right).

A series of convolutional layers is the usual architecture for mapping a large-dimension signal, such as an image or a sound sample, to a low-dimension tensor. This can be used, for instance, to get class scores for classification or a compressed representation. Transposed convolution layers are used the opposite way to build a large-dimension signal from a compressed representation, either to assess that the compressed representation contains enough information to reconstruct the signal or for synthesis, as it is easier to learn a density model over a low-dimension representation. We will revisit this in § 5.2.

4.3 Activation functions

If a network were combining only linear components, it would itself be a linear operator, so it is essential to have non-linear operations. These are implemented in particular with activation functions, which are layers that transform each component of the input tensor individually through a mapping, resulting in a tensor of the same shape.

There are many different activation functions, but the most used is the Rectified Linear Unit (ReLU) [[Glorot et al., 2011](#)], which sets negative values to zero and keeps positive values unchanged (see Figure 4.5, top right):

$$\text{relu}(x) = \begin{cases} 0 & \text{if } x < 0, \\ x & \text{otherwise.} \end{cases}$$

Given that the core training strategy of deep-learning relies on the gradient, it may seem problematic to have a mapping that is not differentiable at zero and constant on half the real line. However, the main property gradient descent requires is that the gradient is informative on average. Parameter initialization and data normalization make half of the activations positive

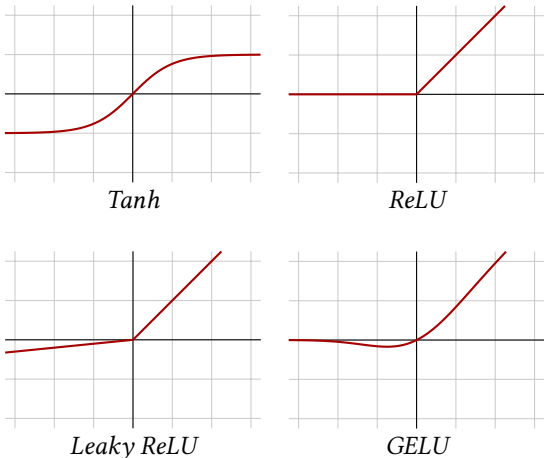


Figure 4.5: Activation functions.

when the training starts, ensuring that this is the case.

Before the generalization of ReLU, the standard activation function was the hyperbolic tangent (Tanh), see Figure 4.5, top left) which saturates exponentially fast on both the negative and positive sides, aggravating the vanishing gradient.

Other popular activation functions follow the same idea of keeping positive values unchanged and squashing the negative values. Leaky ReLU [Maas et al., 2013] applies a small positive multi-

plying factor to the negative values (see Figure 4.5, bottom left):

$$\text{leaky relu}(x) = \begin{cases} ax & \text{if } x < 0, \\ x & \text{otherwise.} \end{cases}$$

And GELU [Hendrycks and Gimpel, 2016] is defined using the cumulative distribution function of the Gaussian distribution, that is:

$$\text{gelu}(x) = xP(Z \leq x),$$

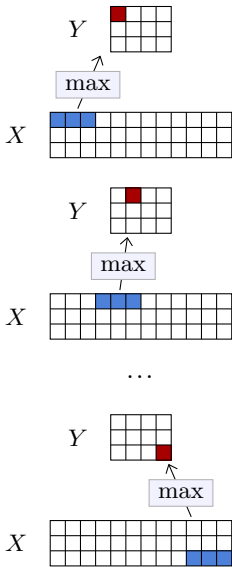
where $Z \sim \mathcal{N}(0, 1)$. It roughly behaves like a smooth ReLU (see Figure 4.5, bottom right).

The choice of an activation function, in particular among the variants of ReLU, is generally driven by empirical performance.

In its standard form, this layer computes the maximum activation per channel, over non-overlapping sub-tensors of spatial size equal to the kernel size. These values are stored in a result tensor with the same number of channels as the input, and whose spatial size is divided by the kernel size. As with the convolution, this operator has three hyper-parameters: padding, stride, and dilation, with the stride being equal to the kernel size by default. A smaller stride to the convolutional layers that compute local scores for the presence of parts, as a way of encoding that at least one instance of a part is present. It loses precise location, making it as a logical disjunction, or, when it follows a series of convolutional layers that compute local scores for the presence of parts, as a way of encoding that at least one instance of a part is present.

A classical strategy to reduce the signal size is to use a pooling operation that combines multiple activations into one that ideally summarizes the information. The most standard operation of this class is the max pooling layer, which, similarly to convolution, can operate in 1D and 2D and is defined by a kernel size.

4.4 Pooling



1D max pooling

Figure 4.6: A *1D max pooling* takes as input a $D \times T$ tensor X , computes the max over non-overlapping $1 \times L$ sub-tensors (in blue) and stores the resulting values (in red) in a $D \times (T/L)$ tensor Y .

invariant to local deformations.

A standard alternative is the average pooling layer that computes the average instead of the maximum over the sub-tensors. This is a linear operation, whereas max pooling is not.

4.5 Dropout

Some layers have been designed to explicitly facilitate training or improve the learned representations.

One of the main contributions of that sort was dropout [Srivastava et al., 2014]. Such a layer has no trainable parameters, but one hyper-parameter, p , and takes as input a tensor of arbitrary shape.

It is usually switched off during testing, in which case its output is equal to its input. When it is active, it has a probability p of setting to zero each activation of the input tensor independently, and it re-scales all the activations by a factor of $\frac{1}{1-p}$ to maintain the expected value unchanged (see Figure 4.7).

The motivation behind dropout is to favor meaningful individual activation and discourage group representation. Since the probability that a group of k activations remains intact through a dropout layer is $(1 - p)^k$, joint representations become unreliable, making the training procedure avoid them. It can also be seen as a noise injection that makes the training more robust.

When dealing with images and 2D tensors, the

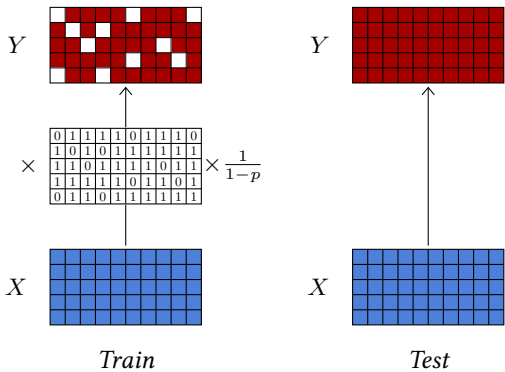


Figure 4.7: *Dropout can process a tensor of arbitrary shape. During training (left), it sets activations at random to zero with probability p and applies a multiplying factor to keep the expected values unchanged. During test (right), it keeps all the activations unchanged.*

short-term correlation of the signals and the resulting redundancy negate the effect of dropout, since activations set to zero can be inferred from their neighbors. Hence, dropout for 2D tensors sets entire channels to zero instead of individual activations (see Figure 4.8).

Although dropout is generally used to improve training and is inactive during inference, it can be used in certain setups as a randomization strategy, for instance, to estimate empirically confidence scores [Gal and Ghahramani, 2015].

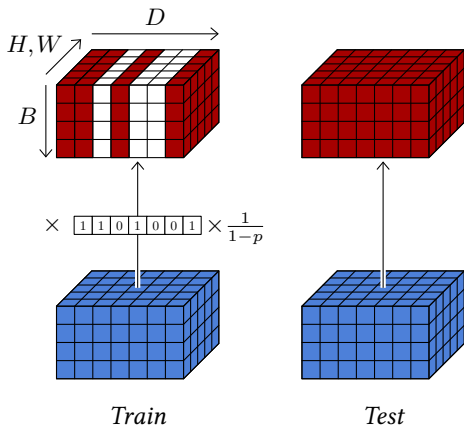


Figure 4.8: 2D signals such as images generally exhibit strong short-term correlation and individual activations can be inferred from their neighbors. This redundancy nullifies the effect of the standard unstructured dropout, so the usual dropout layer for 2D tensors drops entire channels instead of individual values.

4.6 Normalizing layers

An important class of operators to facilitate the training of deep architectures are the normalizing layers, which force the empirical mean and variance of groups of activations.

The main layer in that family is batch normalization [Ioffe and Szegedy, 2015], which is the only standard layer to process batches instead of individual samples. It is parameterized by a hyper-parameter D and two series of trainable scalar parameters β_1, \dots, β_D and $\gamma_1, \dots, \gamma_D$.

Given a batch of B samples x_1, \dots, x_B of dimension D , it first computes for each of the D components an empirical mean \hat{m}_d and variance \hat{v}_d across the batch:

$$\begin{aligned}\hat{m}_d &= \frac{1}{B} \sum_{b=1}^B x_{b,d} \\ \hat{v}_d &= \frac{1}{B} \sum_{b=1}^B (x_{b,d} - \hat{m}_d)^2,\end{aligned}$$

from which it computes for every component $x_{b,d}$ a normalized value $z_{b,d}$, with empirical mean 0 and variance 1, and from it the final result value $y_{b,d}$ with mean β_d and standard de-

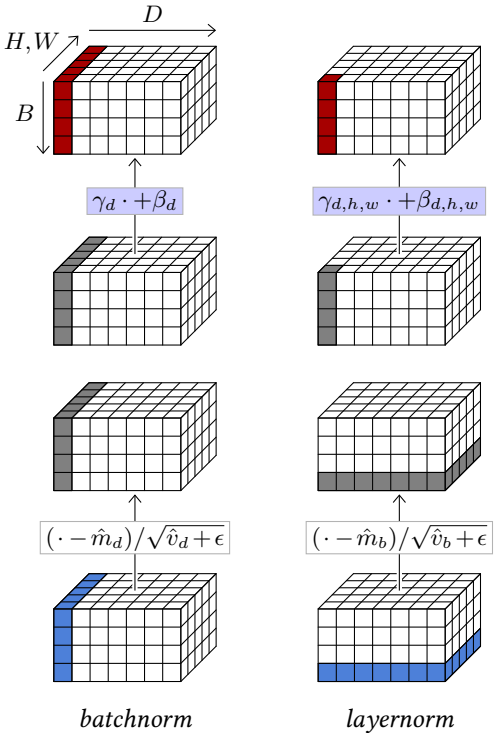


Figure 4.9: *Batch normalization* (left) normalizes in mean and variance each group of activations for a given d , and scales/shifts that same group of activation with learned parameters for each d . *Layer normalization* (right) normalizes each group of activations for a certain b , and scales/shifts each group of activations for a given d, h, w with learned parameters indexed by the same.

viation γ_d :

$$\forall b, \quad z_{b,d} = \frac{x_{b,d} - \hat{m}_d}{\sqrt{\hat{v}_d + \epsilon}} \\ y_{b,d} = \gamma_d z_{b,d} + \beta_d.$$

Because this normalization is defined across a batch, it is done only during training. During testing, the layer transforms individual samples according to the \hat{m}_d s and \hat{v}_d s estimated with a moving average over the full training set, which boils down to a fixed affine transformation per component.

The motivation behind batch normalization was to avoid that a change in scaling in an early layer of the network during training impacts all the layers that follow, which then have to adapt their trainable parameters accordingly. Although the actual mode of action may be more complicated than this initial motivation, this layer considerably facilitates the training of deep models.

In the case of 2D tensors, to follow the principle of convolutional layers of processing all locations similarly, the normalization is done per-channel across all 2D positions, and β and γ remain vectors of dimension D so that the scaling/shift does not depend on the 2D position. Hence, if the tensor to be processed is

of shape $B \times D \times H \times W$, the layer computes (\hat{m}_d, \hat{v}_d) , for $d = 1, \dots, D$ from the corresponding $B \times H \times W$ slice, normalizes it accordingly, and finally scales and shifts its components with the trainable parameters β_d and γ_d .

So, given a $B \times D$ tensor, batch normalization normalizes it across b and scales/shifts it according to d , which can be implemented as a component-wise product by γ and a sum with β . Given a $B \times D \times H \times W$ tensor, it normalizes across b, h, w and scales/shifts according to d (see Figure 4.9, left).

This can be generalized depending on these dimensions. For instance, layer normalization [Ba et al., 2016] computes moments and normalizes across all components of individual samples, and scales and shifts components individually (see Figure 4.9, right). So, given a $B \times D$ tensor, it normalizes across d and scales/shifts also according to the same. Given a $B \times D \times H \times W$ tensor, it normalizes it across d, h, w and scales/shifts according to the same.

Contrary to batch normalization, since it processes samples individually, layer normalization behaves the same during training and testing.

4.7 Skip connections

Another technique that mitigates the vanishing gradient and allows the training of deep architectures are skip connections [Long et al., 2014; Ronneberger et al., 2015]. They are not layers per se, but an architectural design in which outputs of some layers are transported as-is to other layers further in the model, bypassing processing in between. This unmodified signal can be concatenated or added to the input of the layer the connection branches into (see Figure 4.10). A particular type of skip connections are the residual connections which combine the signal with a sum, and usually skip only a few layers (see Figure 4.10, right).

The most desirable property of this design is to ensure that, even in the case of gradient-killing processing at a certain stage, the gradient will still propagate through the skip connections. Residual connections, in particular, allow for the building of deep models with up to several hundred layers, and key models, such as the residual networks [He et al., 2015] in computer vision (see § 5.2), and the Transformers [Vaswani et al., 2017] in natural language processing (see § 5.3), are entirely composed of blocks of layers with residual connections.

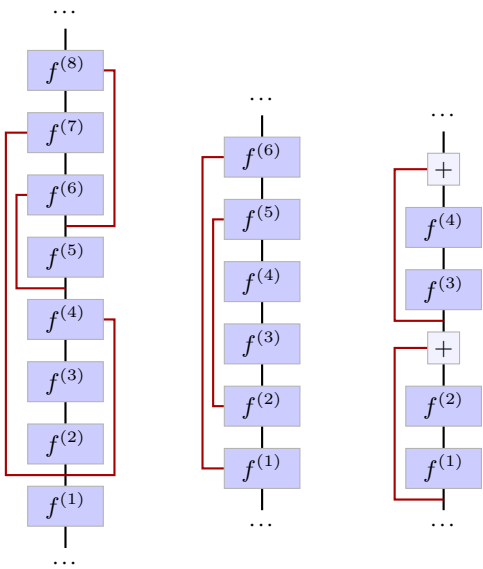


Figure 4.10: *Skip connections, highlighted in red on this figure, transport the signal unchanged across multiple layers. Some architectures (center) that downscale and re-upscale the representation size to operate at multiple scales, have skip connections to feed outputs from the early parts of the network to later layers operating at the same scales [Long et al., 2014; Ronneberger et al., 2015]. The residual connections (right) are a special type of skip connections that sum the original signal to the transformed one, and usually bypass at most a handful of layers [He et al., 2015].*

Their role can also be to facilitate multi-scale reasoning in models that reduce the signal size before re-expanding it, by connecting layers with compatible sizes, for instance for semantic segmentation (see § 6.4). In the case of residual connections, they may also facilitate learning by simplifying the task to finding a differential improvement instead of a full update.

4.8 Attention layers

In many applications, there is a need for an operation able to combine local information at locations far apart in a tensor. For instance, this could be distant details for coherent and realistic image synthesis, or words at different positions in a paragraph to make a grammatical or semantic decision in Natural Language Processing.

Fully connected layers cannot process large-dimension signals, nor signals of variable size, and convolutional layers are not able to propagate information quickly. Strategies that aggregate the results of convolutions, for instance, by averaging them over large spatial areas, suffer from mixing multiple signals into a limited number of dimensions.

Attention layers specifically address this problem by computing an attention score for each component of the resulting tensor to each component of the input tensor, without locality constraints, and averaging the features across the full tensor accordingly [[Vaswani et al., 2017](#)].

Even though they are substantially more complicated than other layers, they have become a standard element in many recent models. They are, in particular, the key building block of Trans-

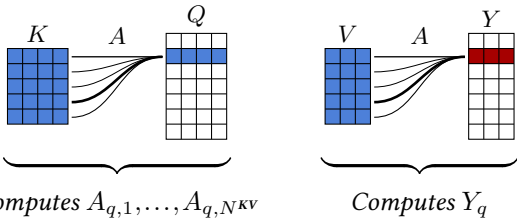


Figure 4.11: The attention operator can be interpreted as matching every query Q_q with all the keys $K_1, \dots, K_{N^{KV}}$ to get normalized attention scores $A_{q,1}, \dots, A_{q,N^{KV}}$ (left, and Equation 4.1), and then averaging the values $V_1, \dots, V_{N^{KV}}$ with these scores to compute the resulting Y_q (right, and Equation 4.2).

formers, the dominant architecture for Large Language Models. See § 5.3 and § 7.1.

Attention operator

Given

- a tensor Q of queries of size $N^Q \times D^{QK}$,
- a tensor K of keys of size $N^{KV} \times D^{QK}$, and
- a tensor V of values of size $N^{KV} \times D^V$,

the attention operator computes a tensor

$$Y = \text{att}(Q, K, V)$$

of dimension $N^Q \times D^V$. To do so, it first computes for every query index q and every key in-

dex k an attention score $A_{q,k}$ as the softargmax of the dot products between the query Q_q and the keys:

$$A_{q,k} = \frac{\exp\left(\frac{1}{\sqrt{D^{QK}}} Q_q \cdot K_k\right)}{\sum_l \exp\left(\frac{1}{\sqrt{D^{QK}}} Q_q \cdot K_l\right)}, \quad (4.1)$$

where the scaling factor $\frac{1}{\sqrt{D^{QK}}}$ keeps the range of values roughly unchanged even for large D^{QK} .

Then a retrieved value is computed for each query by averaging the values according to the attention scores (see Figure 4.11):

$$Y_q = \sum_k A_{q,k} V_k. \quad (4.2)$$

So if a query Q_n matches one key K_m far more than all the others, the corresponding attention score $A_{n,m}$ will be close to one, and the retrieved value Y_n will be the value V_m associated to that key. But, if it matches several keys equally, then Y_n will be the average of the associated values.

This can be implemented as

$$\text{att}(Q, K, V) = \underbrace{\text{softargmax}\left(\frac{QK^\top}{\sqrt{D^{QK}}}\right)}_A V.$$

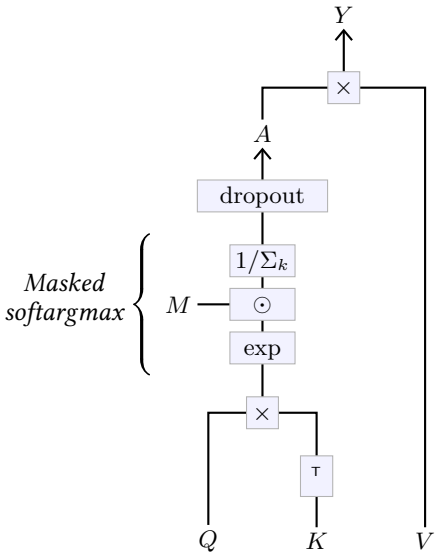


Figure 4.12: The attention operator $Y = \text{att}(Q, K, V)$ computes first an attention matrix A as the per-query softargmax of QK^\top , which may be masked by a constant matrix M before the normalization. This attention matrix goes through a dropout layer before being multiplied by V to get the resulting Y . This operator can be made causal by taking M full of 1s below the diagonal and zeros above.

This operator is usually extended in two ways, as depicted in Figure 4.12. First, the attention matrix can be masked by multiplying it before the softargmax normalization by a Boolean matrix M . This allows, for instance, to make the operator causal by taking M full of 1s below the diagonal and zero above, preventing Y_q from depending on keys and values of indices k greater than q . Second, the attention matrix is processed by a dropout layer (see § 4.5) before being multiplied by V , providing the usual benefits during training.

Since a dot product is computed for every query/key pair, the computational cost of the attention operator is quadratic with the sequence length. This happens to be problematic, as some of the applications of these methods require to process sequences of tens of thousands, or more tokens. Multiple attempts have been made at reducing this cost, for instance by combining a dense attention to a local window with a long-range sparse attention [Beltagy et al., 2020], or linearizing the operator to benefit from the associativity of the matrix product and compute the key-value product before multiplying with the queries [Katharopoulos et al., 2020].

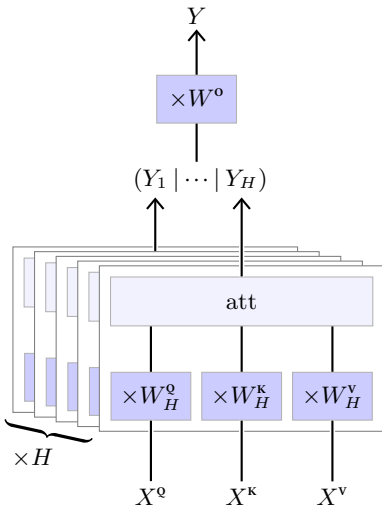


Figure 4.13: *The Multi-head Attention layer applies for each of its $h = 1, \dots, H$ heads a parametrized linear transformation to individual elements of the input sequences X^Q, X^K, X^V to get sequences Q, K, V that are processed by the attention operator to compute Y_h . These H sequences are concatenated along features, and individual elements are passed through one last linear operator to get the final result sequence Y .*

Multi-head Attention Layer

This parameterless attention operator is the key element in the Multi-Head Attention layer depicted in Figure 4.13. The structure of this layer is defined by several hyper-parameters: a number H of heads, and the shapes of three series of H trainable weight matrices

- W^Q of size $H \times D \times D^{QK}$,
- W^K of size $H \times D \times D^{QK}$, and
- W^V of size $H \times D \times D^V$,

to compute respectively the queries, the keys, and the values from the input, and a final weight matrix W^O of size $HD^V \times D$ to aggregate the per-head results.

It takes as input three sequences

- X^Q of size $N^Q \times D$,
- X^K of size $N^{KV} \times D$, and
- X^V of size $N^{KV} \times D$,

from which it computes, for $h = 1, \dots, H$,

$$Y_h = \text{att}(X^Q W_h^Q, X^K W_h^K, X^V W_h^V).$$

These sequences Y_1, \dots, Y_H are concatenated along the feature dimension and each individual element of the resulting sequence is multiplied

by W^o to get the final result:

$$Y = (Y_1 \mid \cdots \mid Y_H)W^o.$$

As we will see in § 5.3 and in Figure 5.6, this layer is used to build two model sub-structures: self-attention blocks, in which the three input sequences X^q , X^k , and X^v are the same, and cross-attention blocks, where X^k and X^v are the same.

It is noteworthy that the attention operator, and consequently the multi-head attention layer when there is no masking, is invariant to a permutation of the keys and values, and equivariant to a permutation of the queries, as it would permute the resulting tensor similarly.

4.9 Token embedding

In many situations, we need to convert discrete tokens into vectors. This can be done with an embedding layer, which consists of a lookup table that directly maps integers to vectors.

Such a layer is defined by two hyper-parameters: the number N of possible token values, and the dimension D of the output vectors, and one trainable $N \times D$ weight matrix M .

Given as input an integer tensor X of dimension $D_1 \times \dots \times D_K$ and values in $\{0, \dots, N-1\}$ such a layer returns a real-valued tensor Y of dimension $D_1 \times \dots \times D_K \times D$ with

$$\forall d_1, \dots, d_K,$$

$$Y[d_1, \dots, d_K] = M[X[d_1, \dots, d_K]].$$

4.10 Positional encoding

While the processing of a fully connected layer is specific to both the positions of the features in the input tensor and to the positions of the resulting activations in the output tensor, convolutional layers and Multi-Head Attention layers are oblivious to the absolute position in the tensor. This is key to their strong invariance and inductive bias, which is beneficial for dealing with a stationary signal.

However, this can be an issue in certain situations where proper processing has to access the absolute positioning. This is the case, for instance, for image synthesis, where the statistics of a scene are not totally stationary, or in natural language processing, where the relative positions of words strongly modulate the meaning of a sentence.

The standard way of coping with this problem is to add or concatenate to the feature representation, at every position, a positional encoding, which is a feature vector that depends on the position in the tensor. This positional encoding can be learned as other layer parameters, or defined analytically.

For instance, in the original Transformer model,

for a series of vectors of dimension D , Vaswani et al. [2017] add an encoding of the sequence index as a series of sines and cosines at various frequencies:

$$\text{pos-enc}[t, d] = \begin{cases} \sin\left(\frac{t}{T^{d/D}}\right) & \text{if } d \in 2\mathbb{N} \\ \cos\left(\frac{t}{T^{(d-1)/D}}\right) & \text{otherwise,} \end{cases}$$

with $T = 10^4$.

Chapter 5

Architectures

The field of deep learning has developed over the years for each application domain multiple deep architectures that exhibit good trade-offs with respect to multiple criteria of interest: e.g. ease of training, accuracy of prediction, memory footprint, computational cost, scalability.

5.1 Multi-Layer Perceptrons

The simplest deep architecture is the Multi-Layer Perceptron (MLP), which takes the form of a succession of fully connected layers separated by activation functions. See an example in Figure 5.1. For historical reasons, in such a model, the number of hidden layers refers to the number of linear layers, excluding the last one.

A key theoretical result is the universal approximation theorem [Cybenko, 1989] which states that, if the activation function σ is continuous

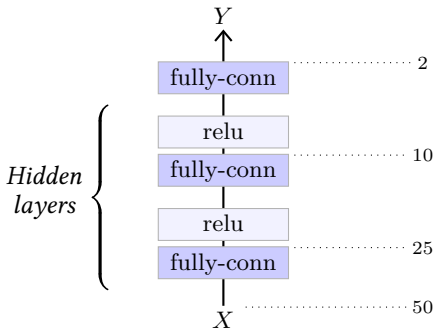


Figure 5.1: This multi-layer perceptron takes as input a one-dimensional tensor of size 50, is composed of three fully connected layers with outputs of dimensions respectively 25, 10, and 2, the two first followed by ReLU layers.

and not polynomial, any continuous function f can be approximated arbitrarily well uniformly on a compact domain, which is bounded and contains its boundary, by a model of the form $l_2 \circ \sigma \circ l_1$ where l_1 and l_2 are affine. Such a model is a MLP with a single hidden layer, and this result implies that it can approximate anything of practical value. However, this approximation holds if the dimension of the first linear layer's output can be arbitrarily large.

In spite of their simplicity, MLPs remain an important tool when the dimension of the signal to be processed is not too large.

5.2 Convolutional networks

The standard architecture for processing images is a convolutional network, or convnet, that combines multiple convolutional layers, either to reduce the signal size before it can be processed by fully connected layers, or to output a 2D signal also of large size.

LeNet-like

The original LeNet model for image classification [[LeCun et al., 1998](#)] combines a series of 2D convolutional layers and max pooling layers that play the role of feature extractor, with a series of fully connected layers which act as a MLP and perform the classification per se (see Figure [5.2](#)).

This architecture was the blueprint for many models that share its structure and are simply larger, such as AlexNet [[Krizhevsky et al., 2012](#)] or the VGG family [[Simonyan and Zisserman, 2014](#)].

Residual networks

Standard convolutional neural networks that follow the architecture of the LeNet family are not easily extended to deep architectures and suffer

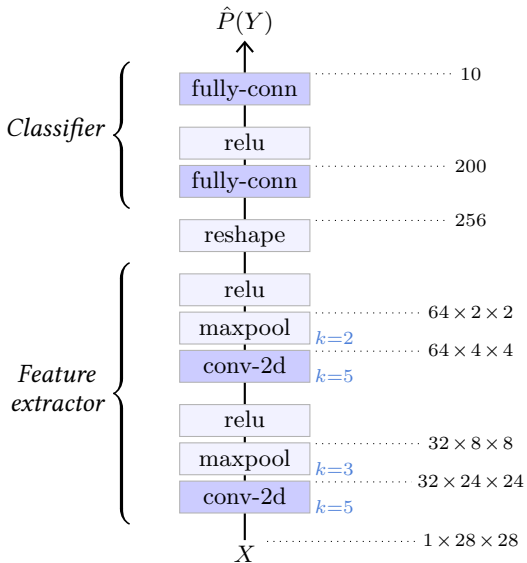


Figure 5.2: Example of a small LeNet-like network for classifying 28×28 grayscale images of handwritten digits [LeCun et al., 1998]. Its first half is convolutional, and alternates convolutional layers per se and max pooling layers, reducing the signal dimension from 28×28 scalars to 256. Its second half processes this 256-dimensional feature vector through a one hidden layer perceptron to compute 10 logit scores corresponding to the ten possible digits.

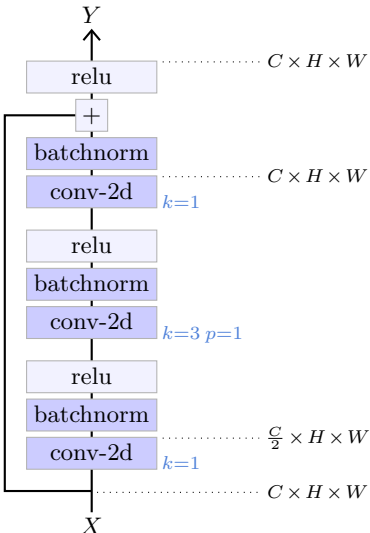


Figure 5.3: A *residual block*.

from the vanishing gradient problem. The residual networks, or ResNets, proposed by He et al. [2015] explicitly address the issue of the vanishing gradient with residual connections (see § 4.7), which allow hundreds of layers. They have become standard architectures for computer vision applications, and exist in multiple versions depending on the number of layers. We are going to look in detail at the architecture of the ResNet-50 for classification.

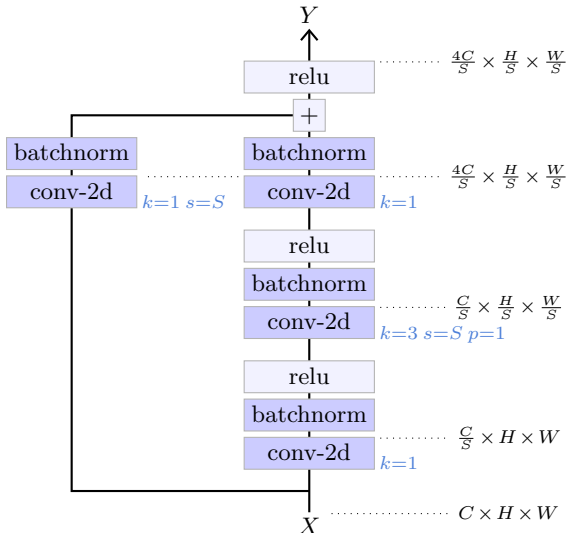


Figure 5.4: A *downscaling residual block*. It admits a hyper-parameter S , the stride of the first convolution layer, which modulates the reduction of the tensor size.

As other ResNets, it is composed of a series of residual blocks, each combining several convolutional layers, batch norm layers, and ReLU layers, wrapped in a residual connection. Such a block is pictured in Figure 5.3.

A key requirement for high performance with real images is to propagate a signal with a large number of channels, to allow for a rich repre-

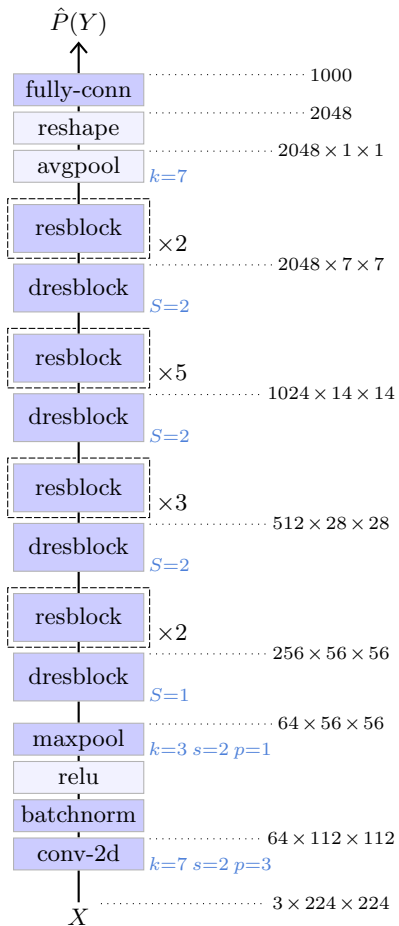


Figure 5.5: *Structure of the ResNet-50 [He et al., 2015]*.

sentation. However, the parameter count of a convolutional layer, and its computational cost, are quadratic with the number of channels. This residual block mitigates this problem by first reducing the number of channels with a 1×1 convolution, then operating spatially with a 3×3 convolution on this reduced number of channels, and then upscaling the number of channels, again with a 1×1 convolution.

The network reduces the dimensionality of the signal to finally compute the logits for the classification. This is done thanks to an architecture composed of several sections, each starting with a downscaling residual block that halves the height and width of the signal, and doubles the number of channels, followed by a series of residual blocks. Such a downscaling residual block has a structure similar to a standard residual block, except that it requires a residual connection that changes the tensor shape. This is achieved with a 1×1 convolution with a stride of two (see Figure 5.4).

The overall structure of the ResNet-50 is presented in Figure 5.5. It starts with a 7×7 convolutional layer that converts the three-channel input image to a 64-channel image of half the size, followed by four sections of residual blocks. Sur-

prisingly, in the first section, there is no downscaling, only an increase of the number of channels by a factor of 4. The output of the last residual block is $2048 \times 7 \times 7$, which is converted to a vector of dimension 2048 by an average pooling of kernel size 7×7 , and then processed through a fully-connected layer to get the final logits, here for 1000 classes.

5.3 Attention models

As stated in § 4.8, many applications, particularly from natural language processing, benefit greatly from models that include attention mechanisms. The architecture of choice for such tasks, which has been instrumental in recent advances in deep learning, is the Transformer proposed by [Vaswani et al. \[2017\]](#).

Transformer

The original Transformer, pictured in Figure 5.7, was designed for sequence-to-sequence translation. It combines an encoder that processes the input sequence to get a refined representation, and an autoregressive decoder that generates each token of the result sequence, given the encoder's representation of the input sequence and the output tokens generated so far.

As the residual convolutional networks of § 5.2, both the encoder and the decoder of the Transformer are sequences of compounded blocks built with residual connections.

- The feed-forward block, pictured at the top of Figure 5.6 is a one hidden layer MLP, preceded by a layer normalization. It can update representations at every position separately.

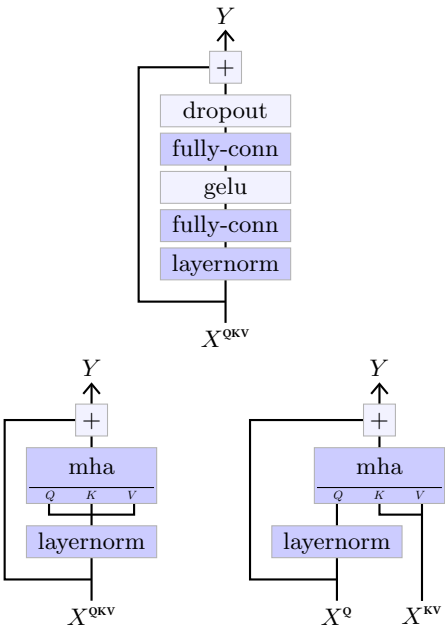


Figure 5.6: Feed-forward block (top), self-attention block (bottom left) and cross-attention block (bottom right). These specific structures proposed by Radford et al. [2018] differ slightly from the original architecture of Vaswani et al. [2017], in particular by having the layer normalization first in the residual blocks.

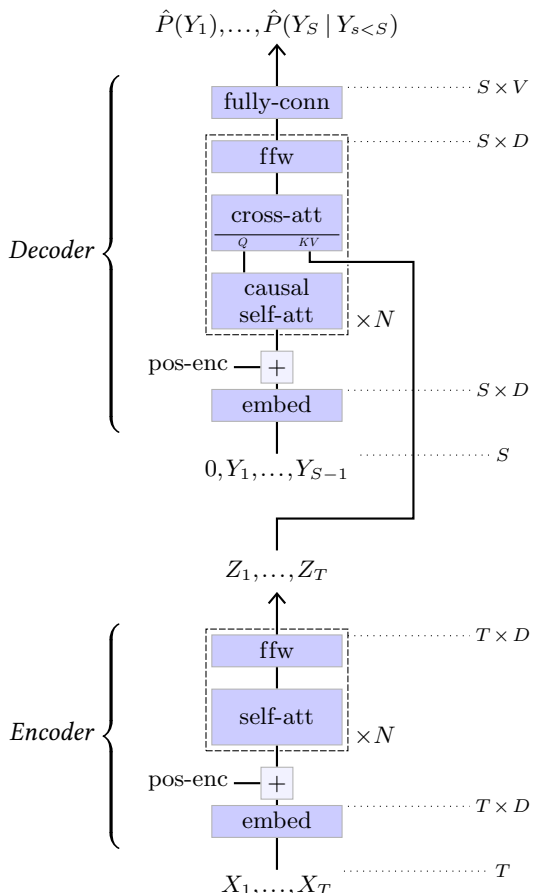


Figure 5.7: *Original encoder-decoder Transformer model for sequence-to-sequence translation [Vaswani et al., 2017].*

- The self-attention block, pictured on the bottom left of Figure 5.6, is a Multi-Head Attention layer (see § 4.8), that recombines information globally, allowing any position to collect information from any other positions, preceded by a layer normalization. This block can be made causal by using an adequate mask in the attention layer, as described in § 4.8
- The cross-attention block, pictured on the bottom right of Figure 5.6, is similar except that it takes as input two sequences, one to compute the queries and one to compute the keys and values.

The encoder of the Transformer (see Figure 5.7, bottom), recodes the input sequence of discrete tokens X_1, \dots, X_T with an embedding layer (see § 4.9), and adds a positional encoding (see § 4.10), before processing it with several self-attention blocks to generate a refined representation Z_1, \dots, Z_T .

The decoder (see Figure 5.7, top), takes as input the sequence Y_1, \dots, Y_{S-1} of result tokens produced so far, similarly recodes them through an embedding layer, adds a positional encoding, and processes it through alternating causal self-attention blocks and cross-attention blocks to

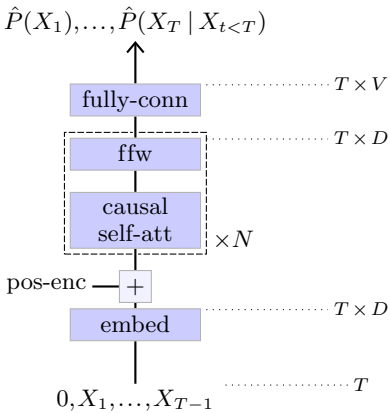


Figure 5.8: *GPT model* [Radford et al., 2018].

produce the logits predicting the next tokens. These cross-attention blocks compute their keys and values from the encoder's result representation Z_1, \dots, Z_T , which allows the resulting sequence to be a function of the original sequence X_1, \dots, X_T .

As we saw in § 3.2 being causal ensures that such a model can be trained by minimizing the cross-entropy summed across the full sequence.

Generative Pre-trained Transformer

The Generative Pre-trained Transformer (GPT) [Radford et al., 2018, 2019], pictured in Figure 5.8

is a pure autoregressive model that consists of a succession of causal self-attention blocks, hence a causal version of the original Transformer encoder.

This class of models scales extremely well, up to hundreds of billions of trainable parameters [[Brown et al., 2020](#)]. We will come back to their use for text generation in § [7.1](#).

Vision Transformer

Transformers have been put to use for image classification with the Vision Transformer (ViT) model [[Dosovitskiy et al., 2020](#)] (see Figure [5.9](#)).

It splits the three-channel input image into M patches of resolution $P \times P$, which are then flattened to create a sequence of vectors X_1, \dots, X_M of shape $M \times 3P^2$. This sequence is multiplied by a trainable matrix W^e of shape $3P^2 \times D$ to map it to an $M \times D$ sequence, to which is concatenated one trainable vector E_0 . The resulting $(M + 1) \times D$ sequence E_0, \dots, E_M is then processed through multiple self-attention blocks. See § [5.3](#) and Figure [5.6](#).

The first element Z_0 in the resultant sequence, which corresponds to E_0 and is not associated with any part of the image, is finally processed

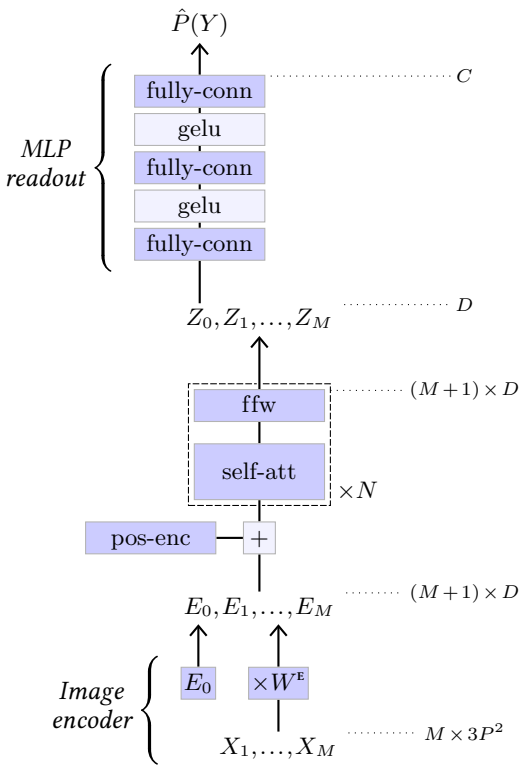


Figure 5.9: *Vision Transformer model [Dosovitskiy et al., 2020]*.

by a two-hidden-layer MLP to get the final C logits. Such a token, added for a readout of a class prediction, was introduced by [Devlin et al. \[2018\]](#) in the BERT model and is referred to as a CLS token.

PART III

APPLICATIONS

Chapter 6

Prediction

A first category of applications, such as face recognition, sentiment analysis, object detection, or speech recognition, requires predicting an unknown value from an available signal.

6.1 *Image denoising*

A direct application of deep models to image processing is to recover from degradation by utilizing the redundancy in the statistical structure of images. The petals of a sunflower in a grayscale picture can be colored with high confidence, and the texture of a geometric shape such as a table on a low-light, grainy picture can be corrected by averaging it over a large area likely to be uniform.

A denoising autoencoder is a model that takes a degraded signal \tilde{X} as input and computes an estimate of the original signal X . For images, it is a convolutional network that may integrate skip-connections, in particular to combine representations at the same resolution obtained early and late in the model, as well as attention layers to facilitate taking into account elements that are far away from each other.

Such a model is trained by collecting a large number of clean samples paired with their degraded inputs. The latter can be captured in degraded conditions, such as low-light or inadequate focus, or generated algorithmically, for instance, by converting the clean sample to grayscale, reducing its size, or aggressively compressing it

with a lossy compression method.

The standard training procedure for denoising autoencoders uses the MSE loss summed across all pixels, in which case the model aims at computing the best average clean picture, given the degraded one, that is $\mathbb{E}[X | \tilde{X}]$. This quantity may be problematic when X is not completely determined by \tilde{X} , in which case some parts of the generated signal may be an unrealistic, blurry average.

6.2 *Image classification*

Image classification is the simplest strategy for extracting semantics from an image and consists of predicting a class from a finite, predefined number of classes, given an input image.

The standard models for this task are convolutional networks, such as ResNets (see § 5.2), and attention-based models such as ViT (see § 5.3). These models generate a vector of logits with as many dimensions as there are classes.

The training procedure simply minimizes the cross-entropy loss (see § 3.1). Usually, performance can be improved with data augmentation, which consists of modifying the training samples with hand-designed random transformations that do not change the semantic content of the image, such as cropping, scaling, mirroring, or color changes.

6.3 Object detection

A more complex task for image understanding is object detection, in which the objective is, given an input image, to predict the classes and positions of objects of interest.

An object position is formalized as the four coordinates (x_1, y_1, x_2, y_2) of a rectangular bounding box, and the ground truth associated with each training image is a list of such bounding boxes, each labeled with the class of the object contained therein.

The standard approach to solve this task, for instance, by the Single Shot Detector (SSD) [[Liu et al., 2015](#)]), is to use a convolutional neural network that produces a sequence of image representations Z_s of size $D_s \times H_s \times W_s$, $s = 1, \dots, S$, with decreasing spatial resolution $H_s \times W_s$ down to 1×1 for $s = S$ (see Figure 6.1). Each of these tensors covers the input image in full, so the h, w indices correspond to a partitioning of the image lattice into regular squares that gets coarser when s increases.

As seen in § 4.2, and illustrated in Figure 4.4, due to the succession of convolutional layers, a feature vector $(Z_s[0, h, w], \dots, Z_s[D_s - 1, h, w])$ is a descriptor of an area of the image, called its

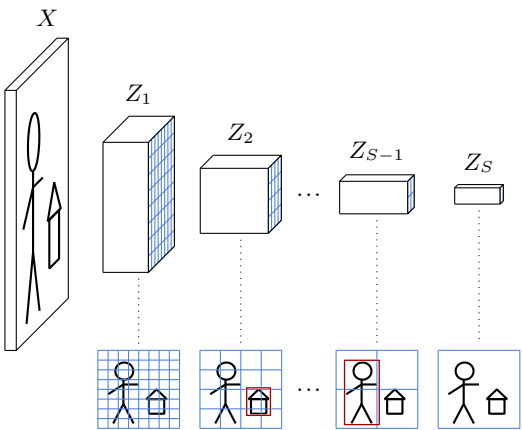


Figure 6.1: A convolutional object detector processes the input image to generate a sequence of representations of decreasing resolutions. It computes for every h, w , at every scale s , a pre-defined number of bounding boxes whose centers are in the image area corresponding to that cell, and whose sizes are such that they fit in its receptive field. Each prediction takes the form of the estimates $(\hat{x}_1, \hat{x}_2, \hat{y}_1, \hat{y}_2)$, represented by the red boxes above, and a vector of $C + 1$ logits for the C classes of interest, and an additional “no object” class.

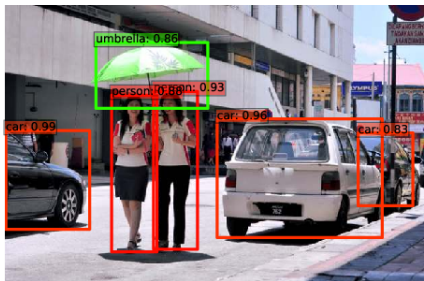
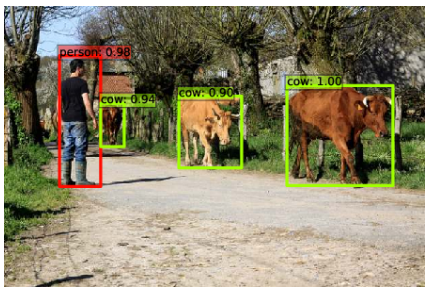
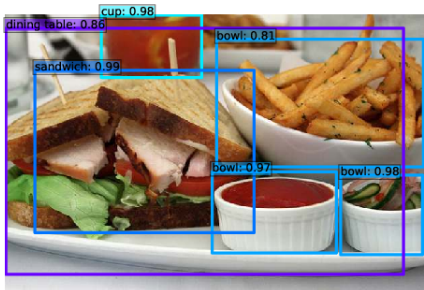


Figure 6.2: Examples of object detection with the Single-Shot Detector [Liu et al., 2015].

receptive field, that is larger than this square but centered on it. This results in a non-ambiguous matching of any bounding box (x_1, x_2, y_1, y_2) to a s, h, w , determined respectively by $\max(x_2 - x_1, y_2 - y_1)$, $\frac{y_1 + y_2}{2}$, and $\frac{x_1 + x_2}{2}$.

Detection is achieved by adding S convolutional layers, each processing a Z_s and computing, for every tensor indices h, w , the coordinates of a bounding box and the associated logits. If there are C object classes, there are $C + 1$ logits, the additional one standing for “no object.” Hence, each additional convolution layer has $4 + C + 1$ output channels. The SSD algorithm in particular generates several bounding boxes per s, h, w , each dedicated to a hard-coded range of aspect ratios.

Training sets for object detection are costly to create, since the labeling with bounding boxes requires a slow human intervention. To mitigate this issue, the standard approach is to fine-tune a convolutional model that has been pre-trained on a large classification dataset such as VGG-16 for the original SSD, and to replace its final fully-connected layers with additional convolutional ones. Surprisingly, models trained for classification only learn feature representations that can be repurposed for object detection, even though

that task involves the regression of geometric quantities.

During training, every ground-truth bounding box is associated with its s, h, w , and induces a loss term composed of a cross-entropy loss for the logits, and a regression loss such as MSE for the bounding box coordinates. Every other s, h, w free of bounding-box match induces a cross-entropy only penalty to predict the class “no object”.

6.4 Semantic segmentation

The finest-grain prediction task for image understanding is semantic segmentation, which consists of predicting, for each pixel, the class of the object to which it belongs. This can be achieved with a standard convolutional neural network that outputs a convolutional map with as many channels as classes, carrying the estimated logits for every pixel.

While a standard residual network, for instance, can generate a dense output of the same resolution as its input, as for object detection, this task requires operating at multiple scales. This is necessary so that any object, or sufficiently informative sub-part, regardless of its size, is captured somewhere in the model by the feature representation at a single tensor position. Hence, standard architectures for this task downscale the image with a series of convolutional layers to increase the receptive field of the activations, and re-upscale it with a series of transposed convolutional layers, or other upscaling methods such as bilinear interpolation, to make the prediction at high resolution.

However, a strict downscaling-upscaling architecture does not allow for operating at a fine

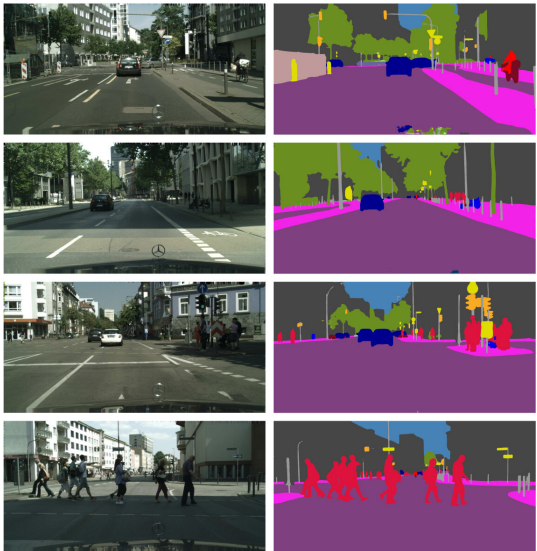


Figure 6.3: *Semantic segmentation results with the Pyramid Scene Parsing Network [Zhao et al., 2016].*

grain when making the final prediction, since all the signal has been transmitted through a low-resolution representation at some point. Models that apply such downscaling-upscaling serially mitigate these issues with skip connections from layers at a certain resolution, before downscaling, to layers at the same resolution, after upscaling [Long et al., 2014; Ronneberger et al., 2015]. Models that do it in parallel, after a convolutional

backbone, concatenate the resulting multi-scale representation after upscaling, before making the final per-pixel prediction [Zhao et al., 2016].

Training is achieved with a standard cross-entropy summed over all the pixels. As for object detection, training can start from a network pre-trained on a large-scale image classification dataset to compensate for the limited availability of segmentation ground truth.

6.5 Speech recognition

Speech recognition consists of converting a sound sample into a sequence of words. There have been plenty of approaches to this problem historically, but a conceptually simple and recent one proposed by Radford et al. [2022] consists of casting it as a sequence-to-sequence translation and then solving it with a standard attention-based Transformer, as described in § 5.3.

Their model first converts the sound signal into a spectrogram, which is a one-dimensional series $T \times D$, that encodes at every time step a vector of energies in D frequency bands. The associated text is encoded with the BPE tokenizer (see § 3.2).

The spectrogram is processed through a few 1D convolutional layers, and the resulting representation is fed into the encoder of the Transformer. The decoder directly generates a discrete sequence of tokens, that correspond to one of the possible tasks considered during training. Multiple objectives are considered: transcription of English or non-English text, translation from any language to English, or detection of non-speech sequences, such as background music or ambient noise.

This approach allows leveraging extremely large datasets that combine multiple types of sound sources with diverse ground truths.

It is noteworthy that even though the ultimate goal of this approach is to produce a translation as deterministic as possible given the input signal, it is formally the sampling of a text distribution conditioned on a sound sample, hence a synthesis process. The decoder is, in fact, extremely similar to the generative model of § [7.1](#).

6.6 *Text-image representations*

A powerful approach to image understanding consists of learning consistent image and text representations, such that an image, or a textual description of it, would be mapped to the same feature vector.

The Contrastive Language-Image Pre-training (CLIP) proposed by Radford et al. [2021] combines an image encoder f , which is a ViT, and a text encoder g , which is a GPT. See § 5.3 for both.

To repurpose a GPT as a text encoder, instead of a standard autoregressive model, they add an “end of sentence” token to the input sequence, and use the representation of this token in the last layer as the embedding. Its dimension is between 512 and 1024, depending on the configuration.

Those two models are trained from scratch using a dataset of 400 million image-text pairs (i_k, t_k) collected from the internet. The training procedure follows the standard mini-batch stochastic gradient descent approach but relies on a contrastive loss. The embeddings are computed for every image and every text of the N pairs in the mini-batch, and a cosine similarity measure is computed not only between text and image em-

beddings from each pair, but also across pairs, resulting in an $N \times N$ matrix of similarity scores:

$$l_{m,n} = f(i_m) \cdot g(t_n), m = 1, \dots, N, n = 1, \dots, N.$$

The model is trained with cross-entropy so that, $\forall n$ the values $l_{1,n}, \dots, l_{N,n}$ interpreted as logit scores predict n , and similarly for $l_{n,1}, \dots, l_{n,N}$. This means that $\forall n, m$, s.t. $n \neq m$ the similarity $l_{n,n}$ is unambiguously greater than both $l_{n,m}$ and $l_{m,n}$.

When it has been trained, this model can be used to do zero-shot prediction, that is, classifying a signal in the absence of training examples by defining a series of candidate classes with text descriptions, and computing the similarity of the embedding of an image with the embedding of each of those descriptions (see Figure 6.4).

Additionally, since the textual descriptions are often detailed, such a model has to capture a richer representation of images and pick up cues beyond what is necessary for instance for classification. This translates to excellent performance on challenging datasets such as ImageNet Adversarial [Hendrycks et al., 2019] which was specifically designed to degrade or erase cues on which standard predictors rely.

Facial Emotion Recognition 2013 (FER2013)

correct label: angry



correct rank: 5/7 correct probability: 8.16%

a photo of a happy looking face.

a photo of a neutral looking face.

a photo of a surprised looking face.

a photo of a fearful looking face.

a photo of a angry looking face.

0 20 40 60 80 100

RESISC45

correct label: roundabout



correct rank: 1/45 correct probability: 96.39%

satellite imagery of roundabout.

satellite imagery of intersection.

satellite imagery of church.

satellite imagery of medium residential.

satellite imagery of chaparral.

0 20 40 60 80 100

UCF101

correct label: Volleyball Spiking



correct rank: 1/101 correct probability: 99.30%

a photo of a person volleyball spiking.

a photo of a person jump rope.

a photo of a person long jump.

a photo of a person soccer penalty.

a photo of a person table tennis shot.

0 20 40 60 80 100

Figure 6.4: The CLIP text-image embedding [Radford et al., 2021] allows for zero-shot prediction by predicting which class description embedding is the most consistent with the image embedding.

6.7 Reinforcement learning

Many problems, such as strategy games or robotic control, can be formalized with a discrete-time state process S_t and reward process R_t that can be modulated by choosing actions A_t . If S_t is Markovian, meaning that it carries alone as much information about the future as all the past states until that instant, such an object is a Markovian Decision Process (MDP).

Given an MDP, the objective is classically to find a policy π such that $A_t = \pi(S_t)$ maximizes the expectation of the return, which is an accumulated discounted reward:

$$\mathbb{E} \left[\sum_{t \geq 0} \gamma^t R_t \right],$$

for a discount factor $0 < \gamma < 1$.

This is the standard setup of Reinforcement Learning (RL), and it can be worked out by introducing the optimal state-action value function $Q(s, a)$ which is the expected return if we execute action a in state s , and then follow the optimal policy. It provides a means to compute the optimal policy as $\pi(s) = \operatorname{argmax}_a Q(s, a)$, and, thanks to the Markovian assumption, it verifies

the Bellman equation:

$$Q(s, a) = \mathbb{E} \left[R_t + \gamma \max_{a'} Q(S_{t+1}, a') \middle| S_t = s, A_t = a \right], \quad (6.1)$$

from which we can design a procedure to train a parametric model $Q(\cdot, \cdot; w)$.

To apply this framework to play classical Atari video games, Mnih et al. [2015] use for S_t the concatenation of the frame at time t and the three that precede, so that the Markovian assumption is reasonable, and use for Q a model dubbed the Deep Q-Network (DQN), composed of two convolutional layers and one fully connected layer with one output value per action, following the classical structure of a LeNet (see § 5.2).

Training is achieved by alternatively playing and recording episodes, and building mini-batches of tuples $(s_n, a_n, r_n, s'_n) \sim (S_t, A_t, R_t, S_{t+1})$ taken across stored episodes and time steps, and minimizing

$$\mathcal{L}(w) = \frac{1}{N} \sum_{n=1}^N (Q(s_n, a_n; w) - y_n)^2 \quad (6.2)$$

with one iteration of SGD, where $y_n = r_n$ if this tuple is the end of the episode, and $y_n = r_n + \gamma \max_a Q(s'_n, a; \bar{w})$ otherwise.

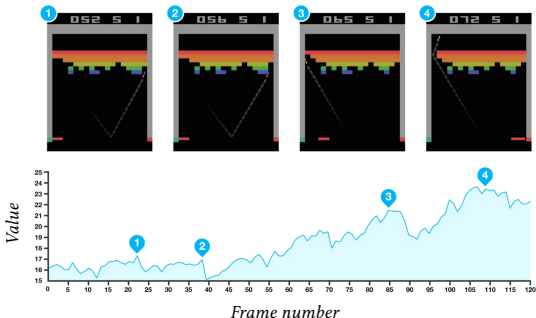


Figure 6.5: This graph shows the evolution of the state value $V(S_t) = \max_a Q(S_t, a)$ during a game of Breakout. The spikes at time points (1) and (2) correspond to clearing a brick, at time point (3) it is about to break through to the top line, and at (4) it does, which ensures a high future reward [Mnih et al., 2015].

Here \bar{w} is a constant copy of w , i.e. the gradient does not propagate through it to w . This is necessary since the target value in Equation 6.1 is the expectation of y_n , while it is y_n itself which is used in Equation 6.2. Fixing w in y_n results in a better approximation of the desirable gradient.

A key issue is the policy used to collect episodes. Mnih et al. [2015] simply use the ϵ -greedy strategy, which consists of taking an action completely at random with probability ϵ , and the optimal action $\text{argmax}_a Q(s, a)$ otherwise. Injecting a bit of randomness is necessary to favor

exploration.

Training is done with ten million frames corresponding to a bit less than eight days of game-play. The trained network computes accurate estimates of the state values (see Figure 6.5), and reaches human performance on a majority of the 49 games used in the experimental validation.

Chapter 7

Synthesis

A second category of applications distinct from prediction is synthesis. It consists of fitting a density model to training samples and providing means to sample from this model.

7.1 *Text generation*

The standard approach to text synthesis is to use an attention-based, autoregressive model. A very successful model proposed by [Radford et al. \[2018\]](#), is the GPT which we described in § 5.3.

This architecture has been used for very large models, such as OpenAI’s 175-billion-parameter GPT-3 [[Brown et al., 2020](#)]. It is composed of 96 self-attention blocks, each with 96 heads, and processes tokens of dimension 12,288, with a hidden dimension of 49,512 in the MLPs of the attention blocks.

When such a model is trained on a very large dataset, it results in a Large Language Model (LLM), which exhibits extremely powerful properties. Besides the syntactic and grammatical structure of the language, it has to integrate very diverse knowledge, e.g. to predict the word following “The capital of Japan is”, “if water is heated to 100 Celsius degrees it turns into”, or “because her puppy was sick, Jane was”.

This results in particular in the ability to solve few-shot prediction, where only a handful of training examples are available, as illustrated in Figure 7.1. More surprisingly, when given a carefully crafted prompt, it can exhibit abil-

I: I love apples, O: positive, I: music is my passion, O: positive, I: my job is boring, O: negative, I: frozen pizzas are awesome, O: **positive**,

I: I love apples, O: positive, I: music is my passion, O: positive, I: my job is boring, O: negative, I: frozen pizzas taste like cardboard, O: **negative**,

I: water boils at 100 degrees, O: physics, I: the square root of two is irrational, O: mathematics, I: the set of prime numbers is infinite, O: mathematics, I: gravity is proportional to the mass, O: **physics**,

I: water boils at 100 degrees, O: physics, I: the square root of two is irrational, O: mathematics, I: the set of prime numbers is infinite, O: mathematics, I: squares are rectangles, O: **mathematics**,

Figure 7.1: *Examples of few-shot prediction with a 120 million parameter GPT model from Hugging Face. In each example, the beginning of the sentence was given as a prompt, and the model generated the part in bold.*

ties for question answering, problem solving, and chain-of-thought that appear eerily close to high-level reasoning [[Chowdhery et al., 2022](#); [Bubeck et al., 2023](#)].

Due to these remarkable capabilities, these models are sometimes called foundation models [[Bommasani et al., 2021](#)].

However, even though it integrates a very large body of knowledge, such a model may be inad-

equate for practical applications, in particular when interacting with human users. In many situations, one needs responses that follow the statistics of a helpful dialog with an assistant. This differs from the statistics of available large training sets, which combine novels, encyclopedias, forum messages, and blog posts.

This discrepancy is addressed by fine-tuning such a language model (see § 3.6). The current dominant strategy is Reinforcement Learning from Human Feedback (RLHF) [Ouyang et al., 2022], which consists of creating small labeled training sets by asking users to either write responses or provide ratings of generated responses. The former can be used as-is to fine-tune the language model, and the latter can be used to train a reward network that predicts the rating and use it as a target to fine-tune the language model with a standard Reinforcement Learning approach.

7.2 *Image generation*

Multiple deep methods have been developed to model and sample from a high-dimensional density. A powerful approach for image synthesis relies on inverting a diffusion process. Such a generative model is referred to, somehow incorrectly, as a diffusion model.

The principle consists of defining analytically a process that gradually degrades any sample, and consequently transforms the complex and unknown density of the data into a simple and well-known density such as a normal, and training a deep architecture to invert this degradation process [Ho et al., 2020].

Given a fixed T , the diffusion process defines a probability distribution over series of $T + 1$ images as follows: sample x_0 uniformly from the dataset, and then sequentially sample $x_{t+1} \sim p(x_{t+1} | x_t), t = 0, \dots, T - 1$, where the conditional distribution p is defined analytically and such that it gradually erases the structure that was in x_0 . The setup should degrade the signal so much that the distribution $p(x_T)$ has a known analytical form which can be sampled.

For instance, Ho et al. [2020] normalize the data to have a mean of 0 and a variance of 1, and their

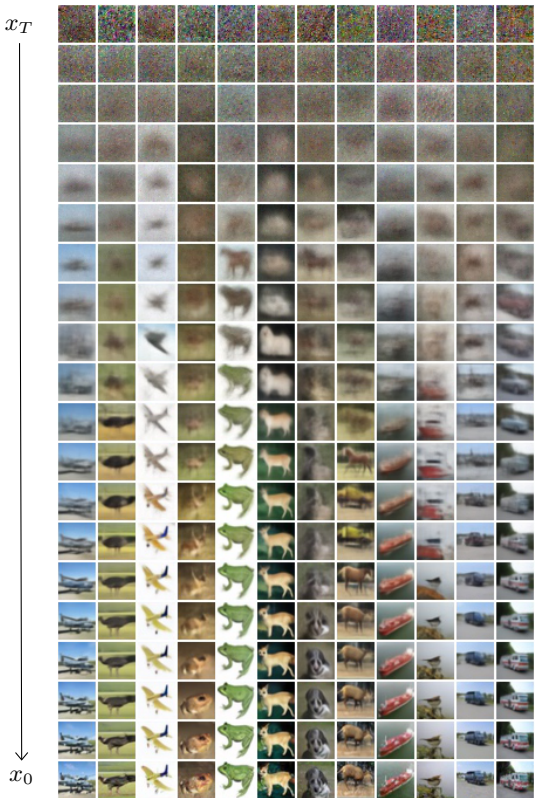


Figure 7.2: *Image synthesis with denoising diffusion [Ho et al., 2020]*. Each sample starts as a white noise x_T (top), and is gradually de-noised by sampling iteratively $x_{t-1} \mid x_t \sim \mathcal{N}(x_t + f(x_t, t; w), \sigma_t)$.

diffusion process consists of adding a bit of white noise and re-normalizing the variance to 1. This process exponentially reduces the importance of x_0 , and x_t 's density can rapidly be approximated with a normal.

The denoiser f is a deep architecture that should model and allow sampling from $f(x_{t-1}, x_t, t; w) \simeq p(x_{t-1} | x_t)$. It can be shown, thanks to a variational bound, that if this one-step reverse process is accurate enough, sampling $x_T \sim p(x_T)$ and denoising T steps with f results in x_0 that follows $p(x_0)$.

Training f can be achieved by generating a large number of sequences $x_0^{(n)}, \dots, x_T^{(n)}$, picking a t_n in each, and maximizing

$$\sum_n \log f\left(x_{t_n-1}^{(n)}, x_{t_n}^{(n)}, t_n; w\right).$$

Given their diffusion process, [Ho et al. \[2020\]](#) have a denoising of the form:

$$x_{t-1} | x_t \sim \mathcal{N}(x_t + f(x_t, t; w); \sigma_t), \quad (7.1)$$

where σ_t is defined analytically.

In practice, such a model initially hallucinates structures by pure luck in the random noise, and

then gradually builds more elements that emerge from the noise by reinforcing the most likely continuation of the image obtained thus far.

This approach can be extended to text-conditioned synthesis, to generate images that match a description. For instance, [Nichol et al. \[2021\]](#) add to the mean of the denoising distribution of Equation 7.1 a bias that goes in the direction of increasing the CLIP matching score (see § 6.6) between the produced image and the conditioning text description.

Chapter 8

The Compute Schism

The scale of deep architectures is critical to their performance and, as we saw in § 3.7, Large Language Models in particular may require amounts of memory and computation that greatly exceed those of consumer hardware.

While training such a model from scratch requires resources available only to large corporations or public bodies, techniques have been developed to allow inference and adaptation to specific tasks under strong resource constraints. Allowing to run models locally instead of through a provider may be highly desirable for cost or confidentiality reasons.

8.1 Prompt Engineering

The simplest strategy to specialize or improve a Large Language Model with a limited computational budget is to use prompt engineering, that is, to carefully craft the beginning of the text sequence to bias the autoregressive process [[Sahoo et al., 2024](#)]. This approach moves a part of the information traditionally encoded in the model’s parameters to the input.

We saw in § [7.1](#) a simple example of few-shot prediction, to use an LLM for a text classification task without fine-tuning. A long and sophisticated prompt allows generalizing this strategy to complex tasks.

Since the prompt’s role is to leverage the “good” biases that were present in the training set, it benefits from surprising strategies such as stating that the response is generated by a skilled professional [[Xu et al., 2023](#)].

The context size of a language model, that is, the number of tokens it can operate on, directly modulates the quantity of information that can be provided in the prompt. This is mostly constrained by the computational cost of standard attention models, which is quadratic with the context size (see § [4.8](#)).

Q: Gina has 105 beans, she gives 23 beans to Bob, and prepares a soup with 53 beans. How many beans are left? A: There are 29 beans left.

Q: I prepare 53 pancakes, eat 5 of them and give 7 to Gina. I then prepare 26 more. How many pancakes are left? A: **27 pancakes are left.**

Q: Gina has 105 beans, she gives 23 beans to Bob, and prepares a soup with 53 beans. How many beans are left? A: Let's proceed step by step: Gina has 105 beans, she gives 23 beans to Bob (82 left), and prepares a soup with 53 beans (29 left). So there are 29 beans left.

Q: I prepare 53 pancakes, eat 5 of them and give 7 to Gina. I then prepare 26 more. How many pancakes are left? A: Let's proceed step by step: **53 pancakes, eat 5 of them (48 left), give 7 to Gina (41 left), prepare 26 more (67 left). So there are 67 pancakes left.**

Figure 8.1: *Example of a chain-of-thought to improve the response of the Llama-3-8B base model. In the two examples, the beginning of the text in normal font is the prompt, and the generated part is indicated in bold. The generation without chain-of-thought (top) leads to an incorrect answer, while the generation with it (bottom) generates a correct answer, by explicitly producing multiple simple arithmetic operations.*

Chain of Thought

A remarkable type of prompting aims at making the model generate intermediate steps before generating the response itself.

Such a chain-of-thought is composed of successive steps that are simpler, hence have been better modeled during training, and are predicted more deterministically [[Wei et al., 2022](#); [Kojima et al., 2022](#)]. See Figure 8.1 for an example.

Retrieval-Augmented Generation

Prompt engineering can also be put to use to connect a language model to an external knowledge base. It plays the role of a smart interface that allows the end user to formulate questions in natural language and get back a response that combines information that is not encoded in the model's parameters [[Lewis et al., 2020](#)].

For such Retrieval-Augmented Generation (RAG), an embedding model is used to retrieve documents whose embedding is correlated to that of the user's query. Then, a prompt is constructed by joining these retrieved documents with instructions to combine them, and the generative model produces the response to the user.

8.2 Quantization

Although training or generating multiple streams can benefit from high-end parallel computing devices, deployment of a Large Language Model for individual use requires generally single-stream inference, which is bounded by memory size and speed far more than by computation.

As stated in § 2.1, parameters, activations, and gradients are usually encoded with 32 or 16 bits. The precision it provides is necessary for training, to allow gradual changes to accumulate.

However, since activations are the sums of many terms, quantization during inference is mitigated by an averaging effect. This is even more true with large architectures, and models quantized down to 6 or 4 bits per parameter exhibit remarkable performance. Additionally to reducing the memory footprint, quantization also improves inference speed significantly.

This has motivated the development of software to quantize existing models with Post-Training Quantization, and run them in single-stream inference on consumer hardware, such as llama.cpp [[Llama.cpp, 2023](#)]. This framework implements multiple formats, that apply specific

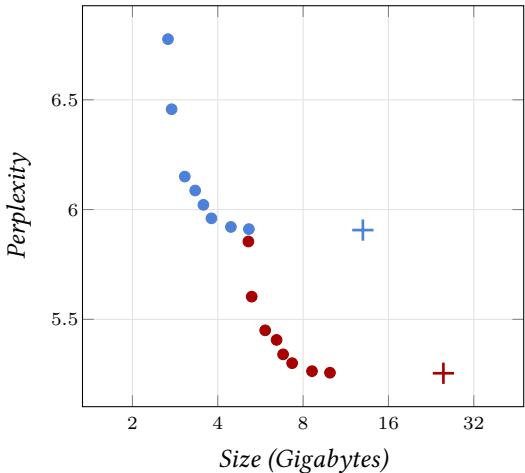


Figure 8.2: *Perplexity* of quantized versions of the language models Llama-7B (blue) and 13B (red) [Touvron et al., 2023] on the wikitext corpus, as a function of the parameters' memory footprint. The crosses are the original FP16 models and the dots correspond to different levels of quantization with `llama.cpp` [Llama.cpp, 2023].

quantization levels for the different weight matrices of a language model. For instance the quantization may use more bits for the W^v weights of the attention blocks, and for the weights of the feed-forward blocks.

An example of `llama.cpp`'s quantization is `Q4_1`.

It quantizes individually sub-blocks of 32 entries of the original weight matrix by storing for each a scaling factor d and a bias m in the original FP16 encoding, and encoding each entry x with 4 bits as a value $q \in \{0, \dots, 2^4 - 1\}$. The resulting de-quantized value being $\tilde{x} = dq + m$.

Such a block was encoded originally as 32 values in FP16, hence 64 bytes, while the quantized version needs 4 bytes for q and m and $32 \cdot 4$ bits = 16 bytes for the entries, hence a total of 20 bytes.

Such an aggressive quantization surprisingly degrades only marginally the performance of the models, as illustrated on Figure 8.2.

An alternative to Post-Training Quantization is Quantization-Aware Training that applies quantization during the forward pass but keeps high-precision encoding of parameters and gradients, and propagates the gradients during the backward pass as if there was no quantization [Ma et al., 2024].

8.3 Adapters

As we saw in § 3.6, fine-tuning is a key strategy to reuse pre-trained models. Since it aims at making only minor changes to an existing model, techniques have been developed that add components with few parameters, referred to as adapters, to the pre-trained architecture, and freeze all the original parameters [Houlsby et al., 2019].

The current dominant method is the Low-Rank Adaptation (LoRA), which adds low-rank corrections to some of the model’s weight matrices [Hu et al., 2021].

Formally, given a linear operation of the form XW^\top , where X is a $N \times D$ tensor of activations for a batch of N samples, and W is a $C \times D$ weight matrix, the LoRA adapter replaces this operation with $X(W + BA)^\top$, where A and B are two trainable matrices of size $R \times D$ and $C \times R$ respectively, with $R \ll \min(C, D)$, and the matrix W is removed from the trainable parameters. The matrix A is initialized with random Gaussian values, and B is set to zero, so that the fine-tuning starts with a model that computes an output identical to that of the original one.

The total number of parameters to optimize with this approach is generally a few percent of the number of parameters in the original model.

The standard procedure to fine-tune a transformer with such adapters is to change only the weight matrices in the attention blocks, and to keep the MLP of the feed-forward blocks unchanged. The same strategy has been used successfully to tune diffusion denoising models by fine-tuning the attention blocks responsible for the text-based conditioning.

Since fine-tuning with LoRA adapters drastically reduces the number of trainable parameters, it reduces the memory footprint required by optimizers such as Adam, which generally store two running average per parameter to optimize. Also, it reduces slightly the computation during the backward pass.

For commercial applications that require a large number of fine-tuned models, the AB pairs can be stored separately from the original model, which has to be stored only once. And finally, contrary to other type of adapters, the modifications can be integrated into the original architecture, simply by adding AB to W , resulting in an architecture and parameter count for inference

strictly identical to that of the base model.

We saw that quantization degrade models' accuracy only marginally. However, gradient descent requires high precision in both the gradient and the trained parameters, to allow the accumulation of small changes. The QLoRA approach combines a quantized base model and unquantized Low-Rank Adaptation to reduce the memory requirement even more [[Dettmers et al., 2023](#)].

8.4 Model merging

An alternative to the fine-tuning and prompting methods seen in the previous sections consists of combining multiple models with diverse capabilities into a single one, without additional training.

Model merging relies on the compatibility between multiple fine-tuned versions of a base model.

[Ilharco et al. \[2022\]](#) showed that models obtained by fine-tuning a CLIP base model on several image classification data-sets can be combined in the parameter space, where they exhibit Task Arithmetic properties.

Formally, let θ be the parameter vector of a pre-trained model, and for $t = 1, \dots, T$, let θ_t and $\tau_t = \theta_t - \theta$ be respectively the parameters after fine-tuning on task t and the corresponding residual. Experiments show that the model with parameters $\theta + \tau_1 + \dots + \tau_T$ exhibits multi-task capabilities. Similarly, subtracting a τ_t degrades the performance on the corresponding task.

Methods have been developed to reduce the interference between the different residuals and improve the performance when the number of

tasks increases [Yadav et al., 2023; Yu et al., 2023].

An alternative to merging models in parameter space is to recombine their layers. Akiba et al. [2024] combine merging the parameters and re-combining layers, and rely on a stochastic optimization to deal with the combinatorial explosion. Experiments with three fine-tuned versions of Mistral-7B [Jiang et al., 2023] show that combining these two merging strategies outperforms both of them.

The Missing Bits

For the sake of concision, this volume skips many important topics, in particular:

Recurrent Neural Networks

Before attention models showed greater performance, Recurrent Neural Networks (RNN) were the standard approach for dealing with temporal sequences such as text or sound samples. These architectures possess an internal hidden state that gets updated each time a component of the sequence is processed. Their main components are layers such as LSTM [[Hochreiter and Schmidhuber, 1997](#)] or GRU [[Cho et al., 2014](#)].

Training a recurrent architecture amounts to unfolding it in time, which results in a long composition of operators. This has historically prompted the design of key techniques now used for deep architectures such as rectifiers and gating, a form of skip connections which are mod-

ulated dynamically.

One of the key drawbacks of traditional recurrent architectures is that the structure of the computation $x_{t+1} = f(x_t)$ imposes to process the input sequence serially, which takes a time proportional to T . In contrast, transformers, for instance, can take advantage of parallel computation, resulting in a constant time if enough computing units are available.

This is addressed by architectures such as QRNN [Bradbury et al., 2016], S4 [Gu et al., 2021], or Mamba [Gu and Dao, 2023], whose recurrent operations are affine so that the f^t themselves, and consequently the $x_t = f^t(x_0)$, can be computed in parallel, resulting in a constant time if f does not depend on t and $\log T$ otherwise, again if enough parallel computing units are available.

Autoencoder

An autoencoder is a model that maps an input signal, possibly of high dimension, to a low-dimension latent representation, and then maps it back to the original signal, ensuring that information has been preserved. We saw it in § 6.1 for denoising, but it can also be used to automatically discover a meaningful low-dimension

parameterization of the data manifold.

The Variational Autoencoder (VAE) proposed by [Kingma and Welling \[2013\]](#) is a generative model with a similar structure. It imposes, through the loss, a pre-defined distribution on the latent representation. This allows, after training, the generation of new samples by sampling the latent representation according to this imposed distribution and then mapping back through the decoder.

Generative Adversarial Networks

Another approach to density modeling is the Generative Adversarial Networks (GAN) introduced by [Goodfellow et al. \[2014\]](#). This method combines a generator, which takes a random input following a fixed distribution as input and produces a structured signal such as an image, and a discriminator, which takes a sample as input and predicts whether it comes from the training set or if it was generated by the generator.

Training optimizes the discriminator to minimize a standard cross-entropy loss, and the generator to maximize the discriminator's loss. It can be shown that, at equilibrium, the gener-

ator produces samples indistinguishable from real data. In practice, when the gradient flows through the discriminator to the generator, it informs the latter about the cues that the discriminator uses that need to be addressed.

Graph Neural Networks

Many applications require processing signals which are not organized regularly on a grid. For instance, proteins, 3D meshes, geographic locations, or social interactions are more naturally structured as graphs. Standard convolutional networks or even attention models are poorly adapted to process such data, and the tool of choice for such a task is Graph Neural Networks (GNN) [[Scarselli et al., 2009](#)].

These models are composed of layers that compute activations at each vertex by combining linearly the activations located at its immediate neighboring vertices. This operation is very similar to a standard convolution, except that the data structure does not reflect any geometrical information associated with the feature vectors they carry.

Self-supervised training

As stated in § 7.1, even though they are trained only to predict the next word, Large Language Models trained on large unlabeled datasets such as GPT (see § 5.3) are able to solve various tasks, such as identifying the grammatical role of a word, answering questions, or even translating from one language to another [Radford et al., 2019].

Such models constitute one category of a larger class of methods that fall under the name of self-supervised learning, and try to take advantage of unlabeled datasets [Balestrieri et al., 2023].

The key principle of these methods is to define a task that does not require labels but necessitates feature representations which are useful for the real task of interest, for which a small labeled dataset exists. In computer vision, for instance, image features can be optimized so that they are invariant to data transformations that do not change the semantic content of the image, while being statistically uncorrelated [Zbontar et al., 2021].

In both NLP and computer vision, a powerful generic strategy is to train a model to recover parts of the signal that have been masked [Devlin

et al., 2018; Zhou et al., 2021].

Bibliography

- T. Akiba, M. Shing, Y. Tang, et al. Evolutionary Optimization of Model Merging Recipes. *CoRR*, abs/2403.13187, 2024. [[pdf](#)]. 157
- J. L. Ba, J. R. Kiros, and G. E. Hinton. Layer Normalization. *CoRR*, abs/1607.06450, 2016. [[pdf](#)]. 83
- R. Balestrieri, M. Ibrahim, V. Sobal, et al. A Cookbook of Self-Supervised Learning. *CoRR*, abs/2304.12210, 2023. [[pdf](#)]. 162
- A. Baydin, B. Pearlmutter, A. Radul, and J. Siskind. Automatic differentiation in machine learning: a survey. *CoRR*, abs/1502.05767, 2015. [[pdf](#)]. 42
- M. Belkin, D. Hsu, S. Ma, and S. Mandal. Reconciling modern machine learning and the bias-variance trade-off. *CoRR*, abs/1812.11118, 2018. [[pdf](#)]. 50

- I. Beltagy, M. Peters, and A. Cohan. Longformer: The Long-Document Transformer. *CoRR*, abs/2004.05150, 2020. [[pdf](#)]. 91
- R. Bommasani, D. Hudson, E. Adeli, et al. On the Opportunities and Risks of Foundation Models. *CoRR*, abs/2108.07258, 2021. [[pdf](#)]. 140
- J. Bradbury, S. Merity, C. Xiong, and R. Socher. Quasi-Recurrent Neural Networks. *CoRR*, abs/1611.01576, 2016. [[pdf](#)]. 159
- T. Brown, B. Mann, N. Ryder, et al. Language Models are Few-Shot Learners. *CoRR*, abs/2005.14165, 2020. [[pdf](#)]. 54, 113, 139
- S. Bubeck, V. Chandrasekaran, R. Eldan, et al. Sparks of Artificial General Intelligence: Early experiments with GPT-4. *CoRR*, abs/2303.12712, 2023. [[pdf](#)]. 140
- T. Chen, B. Xu, C. Zhang, and C. Guestrin. Training Deep Nets with Sublinear Memory Cost. *CoRR*, abs/1604.06174, 2016. [[pdf](#)]. 43
- K. Cho, B. van Merriënboer, Ç. Gülcühre, et al. Learning Phrase Representations using RNN Encoder-Decoder for Statistical Machine Translation. *CoRR*, abs/1406.1078, 2014. [[pdf](#)]. 158

- A. Chowdhery, S. Narang, J. Devlin, et al. PaLM: Scaling Language Modeling with Pathways. *CoRR*, abs/2204.02311, 2022. [[pdf](#)]. 9, 54, 140
- G. Cybenko. Approximation by superpositions of a sigmoidal function. *Mathematics of Control, Signals, and Systems*, 2(4):303–314, December 1989. [[pdf](#)]. 99
- J. Deng, W. Dong, R. Socher, et al. ImageNet: A Large-Scale Hierarchical Image Database. In *Conference on Computer Vision and Pattern Recognition (CVPR)*, 2009. [[pdf](#)]. 51
- T. Dettmers, A. Pagnoni, A. Holtzman, and L. Zettlemoyer. QLoRA: Efficient Finetuning of Quantized LLMs. *CoRR*, abs/2305.14314, 2023. [[pdf](#)]. 155
- J. Devlin, M. Chang, K. Lee, and K. Toutanova. BERT: Pre-training of Deep Bidirectional Transformers for Language Understanding. *CoRR*, abs/1810.04805, 2018. [[pdf](#)]. 54, 115, 162
- A. Dosovitskiy, L. Beyer, A. Kolesnikov, et al. An Image is Worth 16x16 Words: Transformers for Image Recognition at Scale. *CoRR*, abs/2010.11929, 2020. [[pdf](#)]. 113, 114

- K. Fukushima. Neocognitron: A self-organizing neural network model for a mechanism of pattern recognition unaffected by shift in position. *Biological Cybernetics*, 36(4):193–202, April 1980. [[pdf](#)]. 2
- Y. Gal and Z. Ghahramani. Dropout as a Bayesian Approximation: Representing Model Uncertainty in Deep Learning. *CoRR*, abs/1506.02142, 2015. [[pdf](#)]. 78
- X. Glorot and Y. Bengio. Understanding the difficulty of training deep feedforward neural networks. In *International Conference on Artificial Intelligence and Statistics (AISTATS)*, 2010. [[pdf](#)]. 44, 62
- X. Glorot, A. Bordes, and Y. Bengio. Deep Sparse Rectifier Neural Networks. In *International Conference on Artificial Intelligence and Statistics (AISTATS)*, 2011. [[pdf](#)]. 71
- A. Gomez, M. Ren, R. Urtasun, and R. Grosse. The Reversible Residual Network: Backpropagation Without Storing Activations. *CoRR*, abs/1707.04585, 2017. [[pdf](#)]. 43
- I. J. Goodfellow, J. Pouget-Abadie, M. Mirza, et al. Generative Adversarial Networks. *CoRR*, abs/1406.2661, 2014. [[pdf](#)]. 160

- A. Gu and T. Dao. Mamba: Linear-Time Sequence Modeling with Selective State Spaces. *CoRR*, abs/2312.00752, 2023. [[pdf](#)]. [159](#)
- A. Gu, K. Goel, and C. Ré. Efficiently Modeling Long Sequences with Structured State Spaces. *CoRR*, abs/2111.00396, 2021. [[pdf](#)]. [159](#)
- K. He, X. Zhang, S. Ren, and J. Sun. Deep Residual Learning for Image Recognition. *CoRR*, abs/1512.03385, 2015. [[pdf](#)]. [52](#), [84](#), [85](#), [103](#), [105](#)
- D. Hendrycks and K. Gimpel. Gaussian Error Linear Units (GELUs). *CoRR*, abs/1606.08415, 2016. [[pdf](#)]. [73](#)
- D. Hendrycks, K. Zhao, S. Basart, et al. Natural Adversarial Examples. *CoRR*, abs/1907.07174, 2019. [[pdf](#)]. [132](#)
- J. Ho, A. Jain, and P. Abbeel. Denoising Diffusion Probabilistic Models. *CoRR*, abs/2006.11239, 2020. [[pdf](#)]. [142](#), [143](#), [144](#)
- S. Hochreiter and J. Schmidhuber. Long Short-Term Memory. *Neural Computation*, 9(8):1735–1780, 1997. [[pdf](#)]. [158](#)
- N. Houlsby, A. Giurgiu, S. Jastrzebski, et al. Parameter-Efficient Transfer Learning for NLP. *CoRR*, abs/1902.00751, 2019. [[pdf](#)]. [153](#)

- E. Hu, Y. Shen, P. Wallis, et al. LoRA: Low-Rank Adaptation of Large Language Models. *CoRR*, abs/2106.09685, 2021. [[pdf](#)]. 153
- G. Ilharco, M. Ribeiro, M. Wortsman, et al. Editing Models with Task Arithmetic. *CoRR*, abs/2212.04089, 2022. [[pdf](#)]. 156
- S. Ioffe and C. Szegedy. Batch Normalization: Accelerating Deep Network Training by Reducing Internal Covariate Shift. In *International Conference on Machine Learning (ICML)*, 2015. [[pdf](#)]. 80
- A. Jiang, A. Sablayrolles, A. Mensch, et al. Mistral 7B. *CoRR*, abs/2310.06825, 2023. [[pdf](#)]. 157
- J. Kaplan, S. McCandlish, T. Henighan, et al. Scaling Laws for Neural Language Models. *CoRR*, abs/2001.08361, 2020. [[pdf](#)]. 52, 53
- A. Katharopoulos, A. Vyas, N. Pappas, and F. Fleuret. Transformers are RNNs: Fast Autoregressive Transformers with Linear Attention. In *Proceedings of the International Conference on Machine Learning (ICML)*, pages 5294–5303, 2020. [[pdf](#)]. 91
- D. Kingma and J. Ba. Adam: A Method for Stochastic Optimization. *CoRR*, abs/1412.6980, 2014. [[pdf](#)]. 39

- D. P. Kingma and M. Welling. Auto-Encoding Variational Bayes. *CoRR*, abs/1312.6114, 2013. [[pdf](#)]. [160](#)
- T. Kojima, S. Gu, M. Reid, et al. Large Language Models are Zero-Shot Reasoners. *CoRR*, abs/2205.11916, 2022. [[pdf](#)]. [149](#)
- A. Krizhevsky, I. Sutskever, and G. Hinton. ImageNet Classification with Deep Convolutional Neural Networks. In *Neural Information Processing Systems (NIPS)*, 2012. [[pdf](#)]. [8](#), [101](#)
- Y. LeCun, B. Boser, J. S. Denker, et al. Backpropagation applied to handwritten zip code recognition. *Neural Computation*, 1(4):541–551, 1989. [[pdf](#)]. [8](#)
- Y. LeCun, L. Bottou, Y. Bengio, and P. Haffner. Gradient-based learning applied to document recognition. *Proceedings of the IEEE*, 86(11):2278–2324, 1998. [[pdf](#)]. [101](#), [102](#)
- P. Lewis, E. Perez, A. Piktus, et al. Retrieval-Augmented Generation for Knowledge-Intensive NLP Tasks. *CoRR*, abs/2005.11401, 2020. [[pdf](#)]. [149](#)
- W. Liu, D. Anguelov, D. Erhan, et al. SSD: Single Shot MultiBox Detector. *CoRR*, abs/1512.02325, 2015. [[pdf](#)]. [121](#), [123](#)

Llama.cpp. Llama.cpp git repository, June 2023.

[[web](#)]. [150](#), [151](#)

J. Long, E. Shelhamer, and T. Darrell. Fully Convolutional Networks for Semantic Segmentation. *CoRR*, abs/1411.4038, 2014. [[pdf](#)]. [84](#), [85](#), [127](#)

S. Ma, H. Wang, L. Ma, et al. The Era of 1-bit LLMs: All Large Language Models are in 1.58 Bits. *CoRR*, abs/2402.17764, 2024. [[pdf](#)]. [152](#)

A. L. Maas, A. Y. Hannun, and A. Y. Ng. Rectifier nonlinearities improve neural network acoustic models. In *proceedings of the ICML Workshop on Deep Learning for Audio, Speech and Language Processing*, 2013. [[pdf](#)]. [72](#)

V. Mnih, K. Kavukcuoglu, D. Silver, et al. Human-level control through deep reinforcement learning. *Nature*, 518(7540):529–533, February 2015. [[pdf](#)]. [135](#), [136](#)

A. Nichol, P. Dhariwal, A. Ramesh, et al. GLIDE: Towards Photorealistic Image Generation and Editing with Text-Guided Diffusion Models. *CoRR*, abs/2112.10741, 2021. [[pdf](#)]. [145](#)

L. Ouyang, J. Wu, X. Jiang, et al. Training language models to follow instructions with hu-

man feedback. *CoRR*, abs/2203.02155, 2022. [[pdf](#)]. 141

R. Pascanu, T. Mikolov, and Y. Bengio. On the difficulty of training recurrent neural networks. In *International Conference on Machine Learning (ICML)*, 2013. [[pdf](#)]. 44

A. Radford, J. Kim, C. Hallacy, et al. Learning Transferable Visual Models From Natural Language Supervision. *CoRR*, abs/2103.00020, 2021. [[pdf](#)]. 131, 133

A. Radford, J. Kim, T. Xu, et al. Robust Speech Recognition via Large-Scale Weak Supervision. *CoRR*, abs/2212.04356, 2022. [[pdf](#)]. 129

A. Radford, K. Narasimhan, T. Salimans, and I. Sutskever. Improving Language Understanding by Generative Pre-Training, 2018. [[pdf](#)]. 109, 112, 139

A. Radford, J. Wu, R. Child, et al. Language Models are Unsupervised Multitask Learners, 2019. [[pdf](#)]. 112, 162

O. Ronneberger, P. Fischer, and T. Brox. U-Net: Convolutional Networks for Biomedical Image Segmentation. In *Medical Image Computing and Computer-Assisted Intervention*, 2015. [[pdf](#)]. 84, 85, 127

- P. Sahoo, A. Singh, S. Saha, et al. A Systematic Survey of Prompt Engineering in Large Language Models: Techniques and Applications. *CoRR*, abs/2402.07927, 2024. [[pdf](#)]. [147](#)
- F. Scarselli, M. Gori, A. C. Tsoi, et al. The Graph Neural Network Model. *IEEE Transactions on Neural Networks (TNN)*, 20(1):61–80, 2009. [[pdf](#)]. [161](#)
- R. Sennrich, B. Haddow, and A. Birch. Neural Machine Translation of Rare Words with Subword Units. *CoRR*, abs/1508.07909, 2015. [[pdf](#)]. [34](#)
- J. Sevilla, L. Heim, A. Ho, et al. Compute Trends Across Three Eras of Machine Learning. *CoRR*, abs/2202.05924, 2022. [[pdf](#)]. [8, 52, 54](#)
- J. Sevilla, P. Villalobos, J. F. Cerón, et al. Parameter, Compute and Data Trends in Machine Learning, May 2023. [[web](#)]. [55](#)
- K. Simonyan and A. Zisserman. Very Deep Convolutional Networks for Large-Scale Image Recognition. *CoRR*, abs/1409.1556, 2014. [[pdf](#)]. [101](#)
- N. Srivastava, G. Hinton, A. Krizhevsky, et al. Dropout: A Simple Way to Prevent Neural

Networks from Overfitting. *Journal of Machine Learning Research (JMLR)*, 15:1929–1958, 2014. [[pdf](#)]. 77

M. Telgarsky. Benefits of depth in neural networks. *CoRR*, abs/1602.04485, 2016. [[pdf](#)]. 47

H. Touvron, T. Lavril, G. Izacard, et al. LLaMA: Open and Efficient Foundation Language Models. *CoRR*, abs/2302.13971, 2023. [[pdf](#)]. 151

A. Vaswani, N. Shazeer, N. Parmar, et al. Attention Is All You Need. *CoRR*, abs/1706.03762, 2017. [[pdf](#)]. 84, 87, 97, 108, 109, 110

J. Wei, X. Wang, D. Schuurmans, et al. Chain of Thought Prompting Elicits Reasoning in Large Language Models. *CoRR*, abs/2201.11903, 2022. [[pdf](#)]. 149

B. Xu, A. Yang, J. Lin, et al. ExpertPrompting: Instructing Large Language Models to be Distinguished Experts. *CoRR*, abs/2305.14688, 2023. [[pdf](#)]. 147

P. Yadav, D. Tam, L. Choshen, et al. TIES-Merging: Resolving Interference When Merging Models. *CoRR*, abs/2306.01708, 2023. [[pdf](#)]. 157

L. Yu, B. Yu, H. Yu, et al. Language Models are Super Mario: Absorbing Abilities from

Homologous Models as a Free Lunch. *CoRR*, abs/2311.03099, 2023. [[pdf](#)]. 157

J. Zbontar, L. Jing, I. Misra, et al. Barlow Twins: Self-Supervised Learning via Redundancy Reduction. *CoRR*, abs/2103.03230, 2021. [[pdf](#)]. 162

M. D. Zeiler and R. Fergus. Visualizing and Understanding Convolutional Networks. In *European Conference on Computer Vision (ECCV)*, 2014. [[pdf](#)]. 69

H. Zhao, J. Shi, X. Qi, et al. Pyramid Scene Parsing Network. *CoRR*, abs/1612.01105, 2016. [[pdf](#)]. 127, 128

J. Zhou, C. Wei, H. Wang, et al. iBOT: Image BERT Pre-Training with Online Tokenizer. *CoRR*, abs/2111.07832, 2021. [[pdf](#)]. 163

Index

- 1D convolution, 66
- 2D convolution, 66
 - activation, 23, 41
 - function, 71, 99
 - map, 69
 - Adam, 39, 154
 - adapter, 153
 - affine operation, 61
 - artificial neural network, 8, 11
 - attention operator, 88
 - autoencoder, 159
 - denoising, 118
 - Autograd, 42
 - autoregressive model, *see* model, autoregressive
 - average pooling, 76
- backpropagation, 42
- backward pass, 42, 154
- basis function regression, 14
- batch, 21, 38
- batch normalization, 80, 104

Bellman equation, 135
bias vector, 61, 67
BPE, *see* Byte Pair Encoding
Byte Pair Encoding, 34, 129

cache memory, 21
capacity, 16
causal, 32, 90, 111
 model, *see* model, causal
chain rule (derivative), 40
chain rule (probability), 30
chain-of-thought, 140, 149
channel, 23
checkpointing, 43
classification, 18, 26, 101, 120
CLIP, *see* Contrastive Language-Image
 Pre-training
CLS token, 115
computational cost, 43, 91
context size, 147
Contrastive Language-Image Pre-training, 131,
 156
contrastive loss, 27, 131
convnet, *see* convolutional network
convolution, 66
convolutional layer, *see* layer, convolutional
convolutional network, 101
cross-attention block, 94, 109, 111
cross-entropy, 27, 31, 45

data augmentation, 120
deep learning, 8, 11
Deep Q-Network, 135
denoising autoencoder, *see* autoencoder,
 denoising
density modeling, 18
depth, 41
diffusion model, 142
dilation, 67, 74
discriminator, 160
downscaling residual block, 106
downstream task, 50
DQN, *see* Deep Q-Network
dropout, 77, 91

embedding layer, *see* layer, embedding
epoch, 48
equivariance, 67, 94

feed-forward block, 108, 109
few-shot prediction, 139
filter, 66
fine-tune, 124
fine-tuning, 51, 141
flops, 22
forward pass, 41
foundation model, 140
FP32, 22
framework, 23

GAN, *see* Generative Adversarial Networks
GELU, 73
Generative Adversarial Networks, 160
Generative Pre-trained Transformer, 112, 131, 139, 162
generator, 160
GNN, *see* Graph Neural Network
GPT, *see* Generative Pre-trained Transformer
GPU, *see* Graphical Processing Unit
gradient descent, 35, 37, 40, 45
gradient norm clipping, 44
gradient step, 35
Graph Neural Network, 161
Graphical Processing Unit, 8, 20
ground truth, 18

hidden layer, *see* layer, hidden
hidden state, 158
hyper parameter, *see* parameter, hyper
hyperbolic tangent, 72

image processing, 101
image synthesis, 87, 142
inductive bias, 17, 49, 66, 67, 96
invariance, 76, 94, 96, 162

kernel size, 66, 74
key, 88

Large Language Model, 51, 56, 88, 139, 146, 162

layer, 41, 59
attention, 87
convolutional, 66, 74, 87, 96, 101, 104, 121, 126, 129
embedding, 95, 111
fully connected, 61, 87, 96, 99, 101
hidden, 99
linear, 61
Multi-Head Attention, 93, 96, 111
normalizing, 80
reversible, 43
layer normalization, 83, 108, 111
Leaky ReLU, 72
learning rate, 35, 50
learning rate schedule, 50
LeNet, 101, 102
linear layer, *see* layer, linear
LLM, *see* Large Language Model
local minimum, 35
logit, 26, 31
LoRA, *see* Low-Rank Adaptation
loss, 12
Low-Rank Adaptation, 153, 155

machine learning, 11, 17, 18
Markovian Decision Process, 134
Markovian property, 134
max pooling, 74, 101
MDP, *see* Markovian, Decision Process

mean squared error, 14, 26
memory requirement, 43
memory speed, 21
metric learning, 27
MLP, *see* multi-layer perceptron, 154
model, 12
 autoregressive, 30, 31, 139
 causal, 33, 91, 111, 112
 parametric, 12
 pre-trained, 51, 124, 128
model merging, 156
multi-layer perceptron, 45, 99–101, 108

Natural Language Processing, 87
NLP, *see* Natural Language Processing
non-linearity, 71
normalizing layer, *see* layer, normalizing

object detection, 121
overfitting, 17, 48

padding, 67, 74
parameter, 12
 hyper, 13, 35, 48, 66, 67, 74, 93, 95
parametric model, *see* model, parametric
peak performance, 22
Perplexity, 151
perplexity, 31
policy, 134
 optimal, 134

pooling, 74
positional encoding, 96, 111
Post-Training Quantization, 150
posterior probability, 26
pre-trained model, *see* model, pre-trained
prompt, 139, 140
engineering, 147

quantization, 150
Quantization-Aware Training, 152
query, 88

RAG, *see* Retrieval-Augmented Generation
random initialization, 62
receptive field, 68, 69, 124
rectified linear unit, 71, 158
recurrent neural network, 158
regression, 18
Reinforcement Learning, 134, 141
Reinforcement Learning from Human Feedback,
141
ReLU, *see* rectified linear unit
residual
block, 104
connection, 84, 103
network, 47, 84, 103
ResNet-50, 103
Retrieval-Augmented Generation, 149
return, 134

reversible layer, *see* layer, reversible
RL, *see* Reinforcement Learning
RLHF, *see* Reinforcement Learning from Human Feedback
RNN, *see* recurrent neural network

scaling laws, 52
self-attention block, 94, 109, 111
self-supervised learning, 162
semantic segmentation, 86, 126
SGD, *see* stochastic gradient descent
Single Shot Detector, 121
skip connection, 84, 127, 158
softargmax, 26, 89
softmax, 26
speech recognition, 129
SSD, *see* Single Shot Detector
stochastic gradient descent, 38, 45, 52
stride, 67, 74
supervised learning, 19

Tanh, *see* hyperbolic tangent
Task Arithmetic, 156
tensor, 23
tensor cores, 21
Tensor Processing Unit, 21
test set, 48
text synthesis, 139
token, 30

tokenizer, 34, 129
TPU, *see* Tensor Processing Unit
trainable parameter, 12, 23, 52
training, 12
training set, 12, 25, 48
Transformer, 47, 84, 88, 96, 108, 110, 129
transformer, 154
transposed convolution, 69, 126

underfitting, 16
universal approximation theorem, 99
unsupervised learning, 19

VAE, *see* variational, autoencoder
validation set, 48
value, 88
vanishing gradient, 44, 58
variational
 autoencoder, 160
 bound, 144
Vision Transformer, 113, 131
ViT, *see* Vision Transformer
vocabulary, 30

weight, 13
 decay, 28
 matrix, 61

zero-shot prediction, 132

This book is licensed under the [Creative Commons BY-NC-SA 4.0 International License](#).

V1.2–May 19, 2024